


## Article

# Thermal Alteration of Organic Matter in the Contact of a Rift-Related Basaltic Dyke: An Example from the Black Limestone, Wadi Matulla, West Central Sinai, Egypt

Ahmed S. A. A. Abu Sharib <sup>1,\*</sup>, Ali Q. Selim <sup>2</sup>, Mohamed M. Abdel Fattah <sup>1</sup>, Safiya M. Hassan <sup>1</sup>  and Ioan V. Sanislav <sup>3</sup>

<sup>1</sup> Geology Department, Faculty of Science, Beni-Suef University, Beni-Suef 62521, Egypt; fattahshad@yahoo.com (M.M.A.F.); safia\_ma\_2000@yahoo.com (S.M.H.)

<sup>2</sup> Faculty of Earth Sciences, Beni-Suef University, Beni-Suef 62521, Egypt; aliselimq@gmail.com

<sup>3</sup> College of Science and Engineering, James Cook University, Townsville, QLD 4811, Australia; ioan.sanislav@jcu.edu.au

\* Correspondence: aabusharib@science.bsu.edu.eg; Tel.: +20-82-1003278107

Received: 16 March 2019; Accepted: 26 April 2019; Published: 6 May 2019



**Abstract:** In the Wadi Matulla area, central Sinai, Egypt, an asymmetric baked zone having an average width of 103 m was formed on both sides of a sub-aerial rift-related Oligocene basaltic dyke cross-cutting organic matter-bearing chalky limestone of the Upper Cretaceous Sudr Formation. Advection was the significant heat transfer mechanism. Very narrow metamorphic and metasomatic zones are developed in the country rock at the immediate contact with the dyke. The change in the thermal maturation of organic matter is reflected in the differences in values of the total organic carbon (TOC) within the baked zone. Such differences account for the color variation of the snow-white limestone from shades of brown, in the mature to barren samples, to black, in the totally carbonized overmature metamorphic ones. This study presents for the first time the thermal effect of mafic dykes on some exposed organic matter-bearing rocks in the Gulf of Suez (GOS) region, and turns attention to the local maturation of source rocks in contact with rift-related intrusives at a relatively greater burial depth in the rift basin.

**Keywords:** baked zone; organic matter; carbonization; maturation; source rock; thermal alteration; Wadi Matulla; Sinai; Egypt

## 1. Introduction

Transformation of organic matter into oil, gas, or graphite depends upon the conditions of temperature and pressure to which the organic matter-bearing sediments/rocks are subjected, the burial rate of the sediments, and the composition and type of the organic matter [1–4]. Among these factors, the time–temperature burial history of the organic matter-bearing sediments/rocks is of prime importance. Slow rate of heating for a long duration at a convenient temperature (approximately 60–225 °C) favors source rock maturation to produce oil and/or gas [1]. On the other hand, conditions of fast rate of heating and/or excessive temperature (approximately >300 °C), such as the heat emanating from a nearby magmatic body, may lead directly to the carbonization and/or graphitization of the organic matter [5,6]. The depth of intrusion, water content, and composition of the magmatic body, and the petrophysical properties such as porosity, permeability, and thermal conductivity of the country rock play a significant role in controlling the degree of organic matter transformation.

The Oligo-Miocene Gulf of Suez (GOS) Rift (Figure 1), Egypt, is associated with widespread volcanic activity in the form of mafic dykes and sills intruding mainly pre-rift, and less commonly syn-rift, successions together with a few flows [7–9]. In the Wadi Matulla area, the eastern side of the GOS, a rift-related basaltic dyke intrudes into the Upper Cretaceous fossiliferous chalky limestone beds of the Sudr Formation (Figure 2). An asymmetric thermally affected zone is developed on both sides of the dyke where the snow-white chalky limestone turns into shades of grey or black. The thermally affected chalky limestone has variable total organic carbon (TOC) contents, some of which, according to Peters’s classification of source rock (1986), nominate the limestone to have a good to very good source rock potential [10].

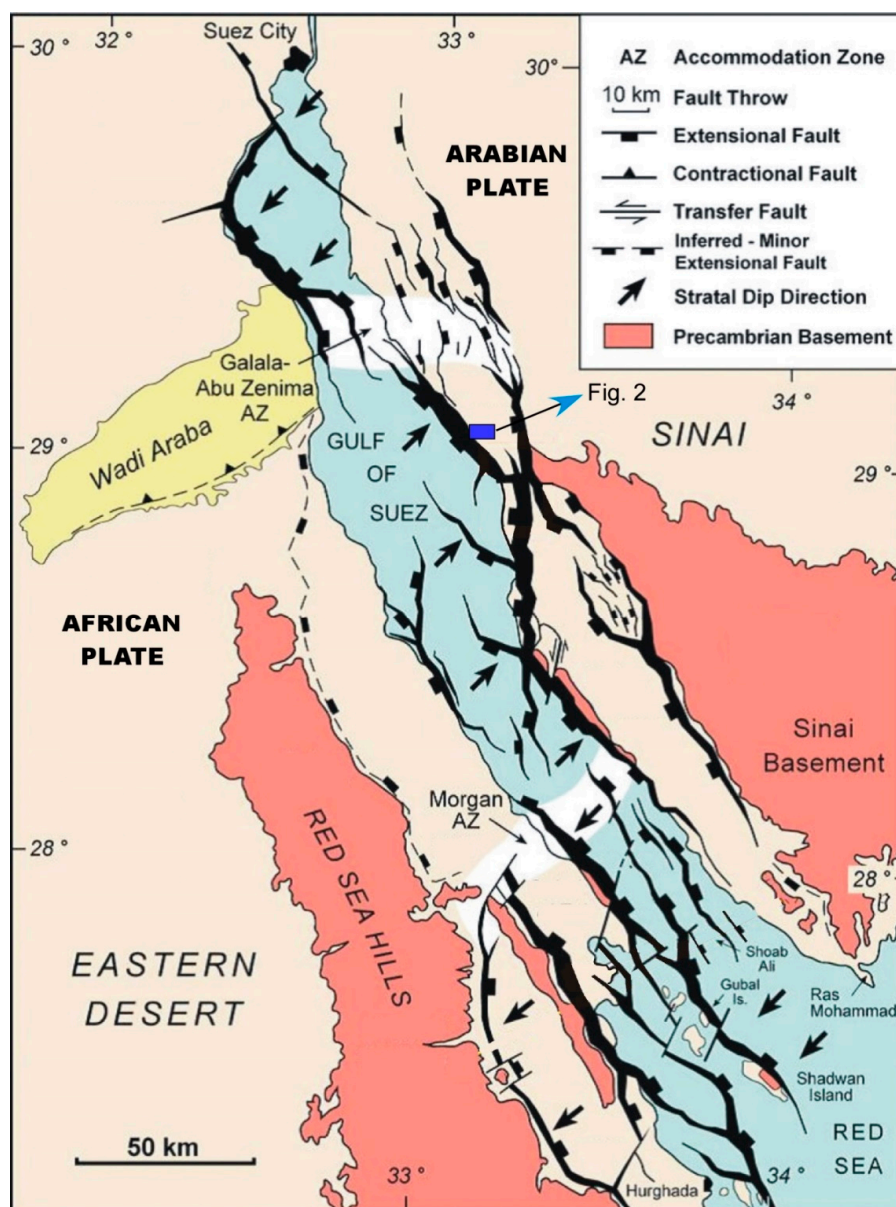


**Figure 1.** A general structural map showing the major faults and the dip polarity along the Gulf of Suez (GOS) Rift. The general stratal dip direction in the northern, southern, and central provinces change from SW to NE and back to SW, respectively, across the Galala-Abu Zenima and Morgan accommodation zones (modified after Bosworth, 2015 [11]). Location of the study area is shown by the small blue rectangle labeled Figure 2.

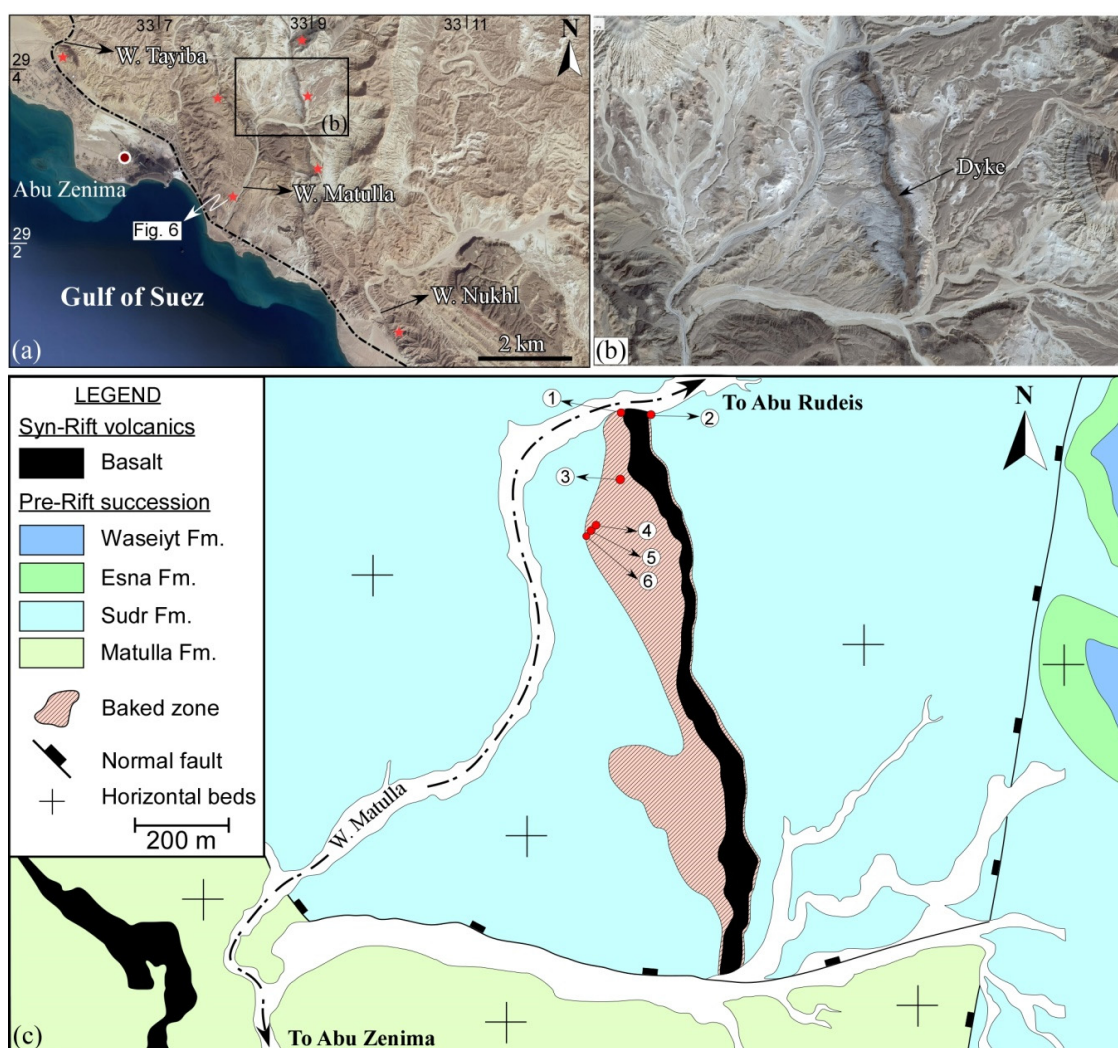


**Figure 2.** (a) A Google Earth map showing the location of the study area (inset labeled Figure 2 in Figure 1), and the distribution of some Tertiary basalt in and outside the study area (marked by red stars). (b) A close-up view of the study area (inset (b) in (a)). (c) A geologic map of (b) showing the extension of the NNW-trending dyke, the major faults, and the different rock units cropping out in the study area. Red circles refer to the number and location of the collected samples. Fm., Formation.

The intriguing topic that addresses the role of igneous activity in the maturation of the country rocks in producing an extractable quantity of hydrocarbons with economic potential has been, and still is, the subject of abundant literature for decades [12–36]. Analogue models of rift-related igneous activity and its impact on the formation of hydrocarbon deposits at the local scale paved the way and were the motive for the present study, which presents, for the first time, the thermal effect of a rift-related dyke on rocks that possess source rock potentials in the Gulf of Suez region.

The purpose of this research is the following: (1) study the thermal effect of the basaltic dyke on the Upper Cretaceous chalky limestone beds of the Sudr Formation, (2) measure the change in the total organic carbon (TOC) in the thermally affected zone on both sides of the dyke, (3) demonstrate the color change in the thermally affected zone, and unravel the reason beyond the coloration in the baked zone, and (4) shed light on the local maturation potential of source rock prone formations in the contact of sills and dykes at a relatively greater burial depth in the Gulf of Suez region.



## 2. Geologic Setting

The Gulf of Suez (GOS) is an elongated 300 km long intra-continental Neogene rift basin that represents the extension of the NW–SE-trending Red Sea rift system. The rifting initiated in the Late Oligocene to Miocene times due to the northeast movement of the Arabian plate relative to the African plate [37–39]. The GOS displays the classical rift geometry that is delineated on both margins by extensional fault systems that define classic half-graben style and rotated fault-blocks [37,40–43]. The master and subsidiary faults link up in a characteristic zigzag shape, which resulted from the interaction between the NNW-, N- and NNE-trending fault segments. The dip polarity of the block-bounding faults changes along the rift axis, dividing the rift into three dip provinces. The blocks of the northern and southern provinces are dominated by NE-dipping master faults, and SW-dipping strata, whereas the strata in the blocks of the central province are tilted due NE, and dragging on the SW-dipping faults (Figure 1). The boundaries between the three dip provinces are transitional through two major accommodation zones: the Galala-Abu Zenima in the north and the Morgan in the south (Figure 1) [37,44–48]. The sedimentary rocks exposed along the GOS Rift's flanks are classified into pre-, syn-, and post-rift successions with reference to the regional faulting [7,8,49].

### 2.1. Rift-Related Volcanic Activity: Sub-Aerial vs. Sub-Aqueous Volcanicity

Intraplate, rift-related Oligocene volcanic activity, in the form of mafic sills, dykes, and a few flows (Figure 2a), are widespread along both sides of the GOS Rift. The dykes vary in orientation from N–S, NNW–SE to NW–SE. On the Sinai side, the Tertiary volcanics intrude pre-rift Precambrian (Gabal Abu Durba) and Phanerozoic (e.g., in the Wadi Tayiba, Wadi Matulla, and Wadi Nukhul) rocks [7–9,50–52]. The volcanics are basaltic in composition (commonly olivine-bearing) with alkaline and transitional tholeiitic geochemical characters [9,52].

The surface outcrops of the Oligocene rocks in Egypt are represented mainly by continental clastic facies ([53], and references therein). In the Wadi Tayiba, about 3–4 km west to west-north-west of the study area (Figure 2a), the clastic-dominated Tayiba red beds unconformably overly the Late Eocene Tanka Formation, and are overlain by rift-related basaltic flow. The beds were interpreted to represent lake deposits that were deposited in areas with low relief [8,53]. In the type locality, the red beds are differentiated into three units: lower calcareous-dominated; middle clastic-dominated red beds; and upper volcanoclastic-dominated [7]. They interpreted the middle and upper units to represent the continental facies that accompanied the initial stage of the Gulf of Suez Rift. A basaltic sill and its associated pyroclastics have been described between the red beds and the overlying basal Miocene clastics [7].

### 2.2. The Study Area

#### Structural and Stratigraphic Framework

The study area (central part of Wadi Matulla) is located ~7 km east-northeast of Abu Zenima city, west-central Sinai (Figures 1 and 2a). It is a part of the Hammam Faraun block that is located within the central dip province of the GOS Rift (Figure 1). The block (Figure 3a), a crustal-scale that is 20 km wide and 40 km long, half-graben, is bounded to the east and west by the steeply dipping (60–80°) Thal and Hammam Faraun faults, respectively [46,54,55]. The block between the two master faults is broken up by multiple subsidiary NW–SE-oriented extensional faults (Figure 3a). The Thal fault is a basement-involved rift-bounding fault juxtaposing the basement rocks on the rift shoulder against the pre- and syn-rift successions in the down faulted block (Figure 3a). On the other hand, Hammam Faraun is a coastal fault juxtaposing a footwall of pre- and syn-rift rocks against the Gulf of Suez to the west (Figure 3a). In the study area, rift-related meso- to macroscopic structural elements are very common. These include extensional faults (Figure 3b), shear fractures (Figure 3c), tension fractures (Figure 3d), and folds in damage zones.



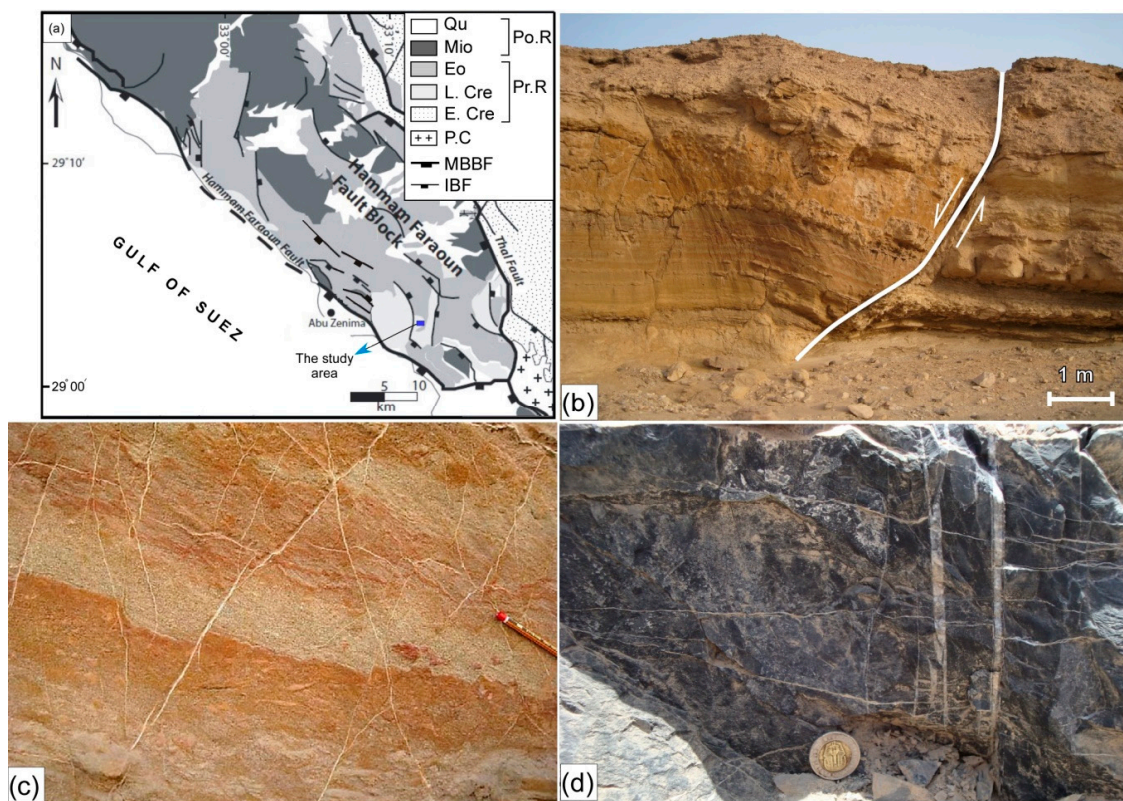


**Figure 3.** (a) A generalized structural map of the Hammam Faraun Fault Block (modified after Bastesen et al., 2015 [56]). (b) N70W-trending flat and ramp listric fault cut through the Matulla Formation. Note the ramp and flat segments of the fault, the rollover anticline and the hangingwall deformation and the footwall duplex. View is to the NW. (c) Conjugate calcite-filled shear fractures showing minor displacements, and well-developed step and graben geometries. Pencil is 12 cm long. (d) Black limestone dissected by two perpendicular sets of fractures. The vertical fractures are variably sized and filled with calcite. The coin diameter is 2.5 cm. (QU: Quaternary; Mio: Miocene; Eo: Eocene; L. Cre: Late Cretaceous; E. Cre: Early Cretaceous; Po. R: Post-Rift; Pr. R: Pre-Rift).

Stratigraphically, the area exposes two lithostratigraphic units of the pre-rift period separated by an unconformity. The lower stratigraphic unit (270–300 m) is represented by a Late Cretaceous succession comprising an older Matulla Formation (Coniacian-Santonian) and a younger Sudr Formation (Campanian-Maastrichtian). The upper stratigraphic unit (250–350 m) comprises the Esna Formation (Danian-Thanatian) at the bottom and the Waseiyt Formation (Yepresian) at the top.

The Matulla Formation comprises a clastic-dominated lower part that is composed mainly of sandstones and shales with a few limestone intercalations, a middle part that is composed of intercalations of sandstone and oolitic limestone, and a carbonate-dominated upper part composed of dolomitic limestone and shale with thin sandstone interbeds. The Sudr Formation is composed of a succession of thinly to thickly bedded snow-white chalky limestone intercalated with yellowish-white marly limestone, and contains brownish-black continuous and discontinuous chert bands, which are very common in the upper part of the succession (Figure 4a). Together with the lower Matulla Formation, it is intensively fractured, dissected by variably oriented calcite and gypsum veinlets (Figure 3c,d), and contains iron concretions that are concentrated along the bedding planes (Figure 4b). Faults cutting through the Sudr Formation are also recorded. The limestone beds are fossiliferous with a few macro fossils (e.g., *Pecten farafarensis*, *Pycnodonte vesicularis*). The Esna Formation, which rests paraconformably on the Sudr Formation, is predominantly made up of a thick section of well-bedded, fissile, olive-green to grey, slope-forming shales with thin ledges of carbonate intercalations in the middle part. The shales are intensively dissected by secondary gypsum, and show ferruginous

mudstone concretions. The Waseiyt Formation conformably overlies the Esna Formation. It is made up of hard fossiliferous limestone with characteristic thin chert bands and nodules in the lower part, dolomitic and chalky limestone in the middle part, and conglomeratic and fossiliferous limestone beds in the upper part. A generalized stratigraphic section of the study area is shown in Figure 5.

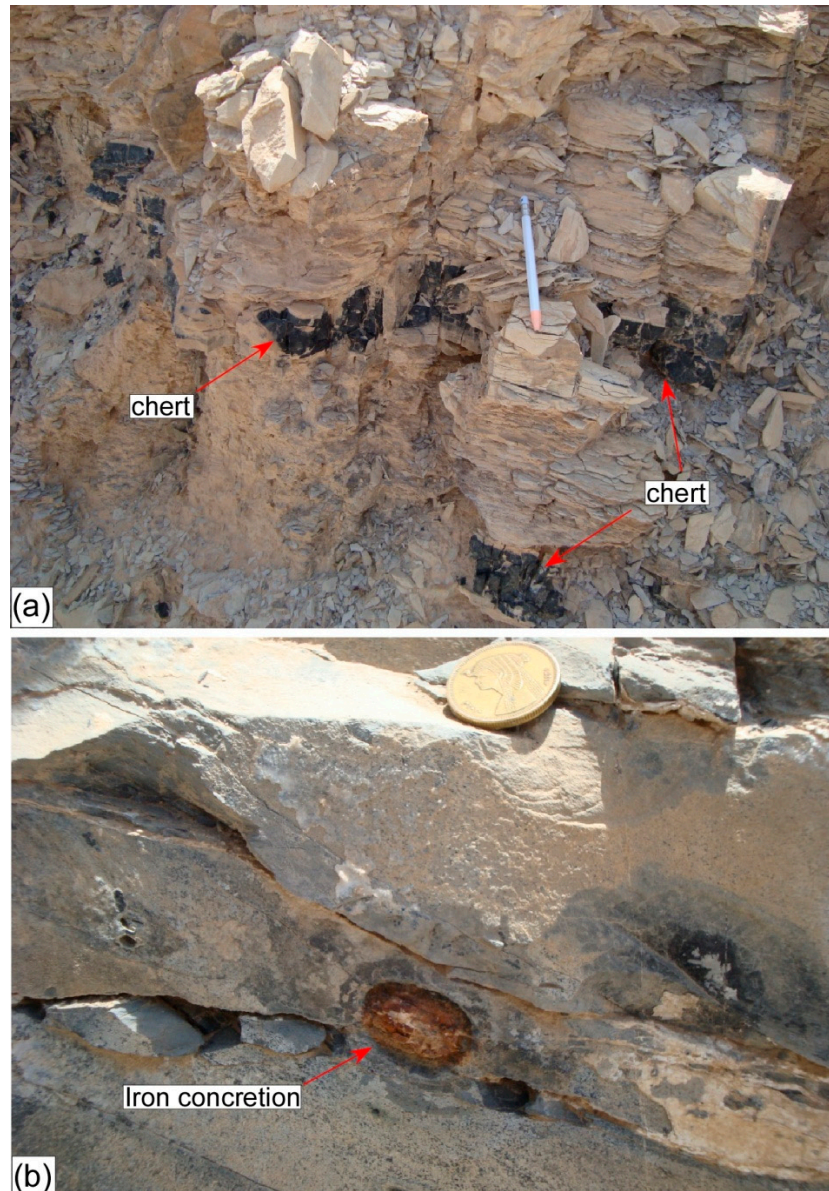


**Figure 4.** (a) Thinly laminated marly limestone with discontinuous chert bands. Pencil is 15 cm long. (b) Iron concretion developed along the bedding plane of black limestone in the baked zone. Coin diameter is 2 cm.

For a detailed bio- and lithostratigraphy of the study area, the reader is referred to Barakat et al., (1988), Abu Khadra et al., (1990), Abdelhamid (1997), Abdel-Gawad (1999), Kora et al., (2002), Shahin (2005), Farouk (2014) [57–63].



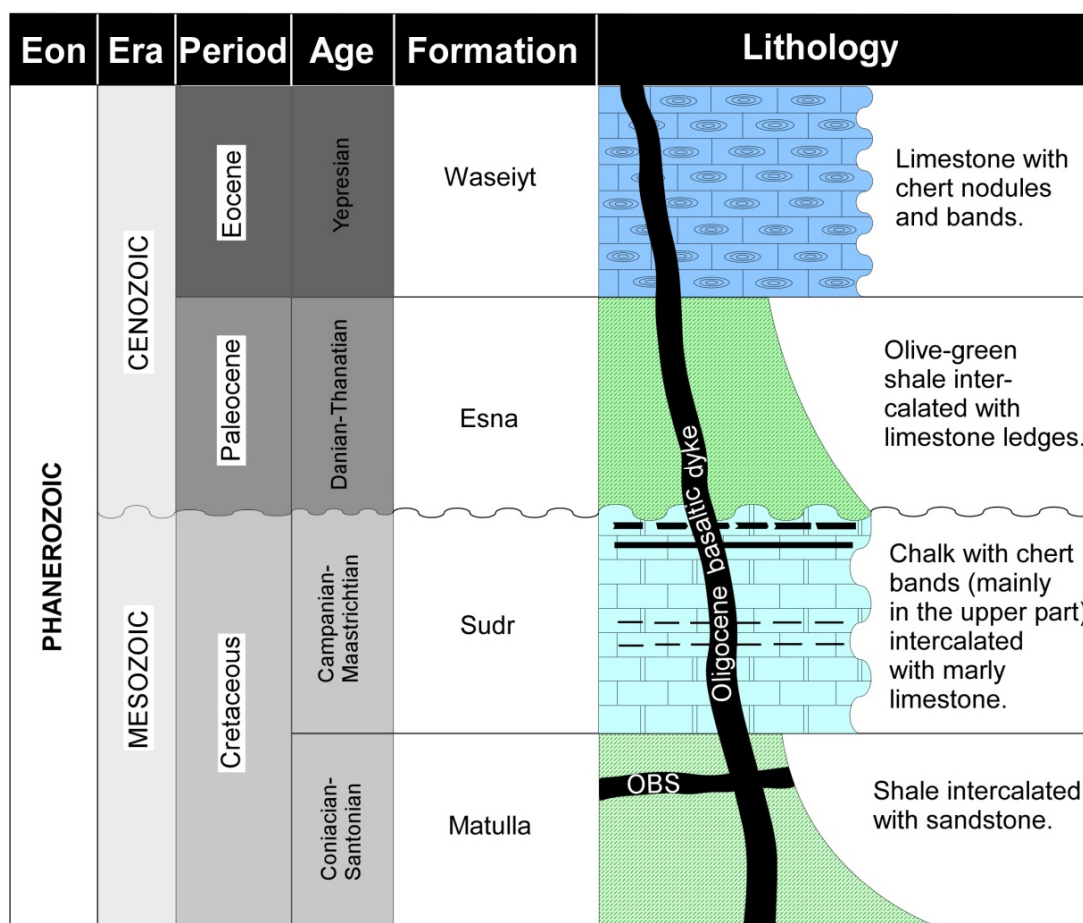


**Figure 5.** A generalized lithostratigraphic section of the study area. (OBS: Oligocene basaltic sill).

In the Wadi Matulla area, a NNW-trending basaltic dyke having an average outcrop width of ~35 m cuts across the Upper Cretaceous Sudr Formation (Figure 2). It extends for about 1.3 km within the study area, and continues north-and southwards, for a considerable distance, outside the study area where it cuts through the Sudr and Matulla Formations, respectively. Geochronological data, based on K/Ar age dating, yielded  $24 \pm 1$  Ma for the dyke [64]. At the entrance of the Wadi Matulla, a ~2 m thick Oligocene basaltic sill having a well-developed columnar jointing intrudes the horizontally bedded Matulla Formation (Figure 6a,b), and confirms the sub-aerial nature of the Oligocene basaltic dyke.

Apart from the rift-related Tertiary volcanics, in and outside the study area, the only recorded igneous rocks are located about 40 km east-southeast from the study area, and belong to the Precambrian basement (Figures 1 and 3). Similarly, the only exposed metamorphic rocks belong to the Precambrian massif of Sinai (Figure 1).



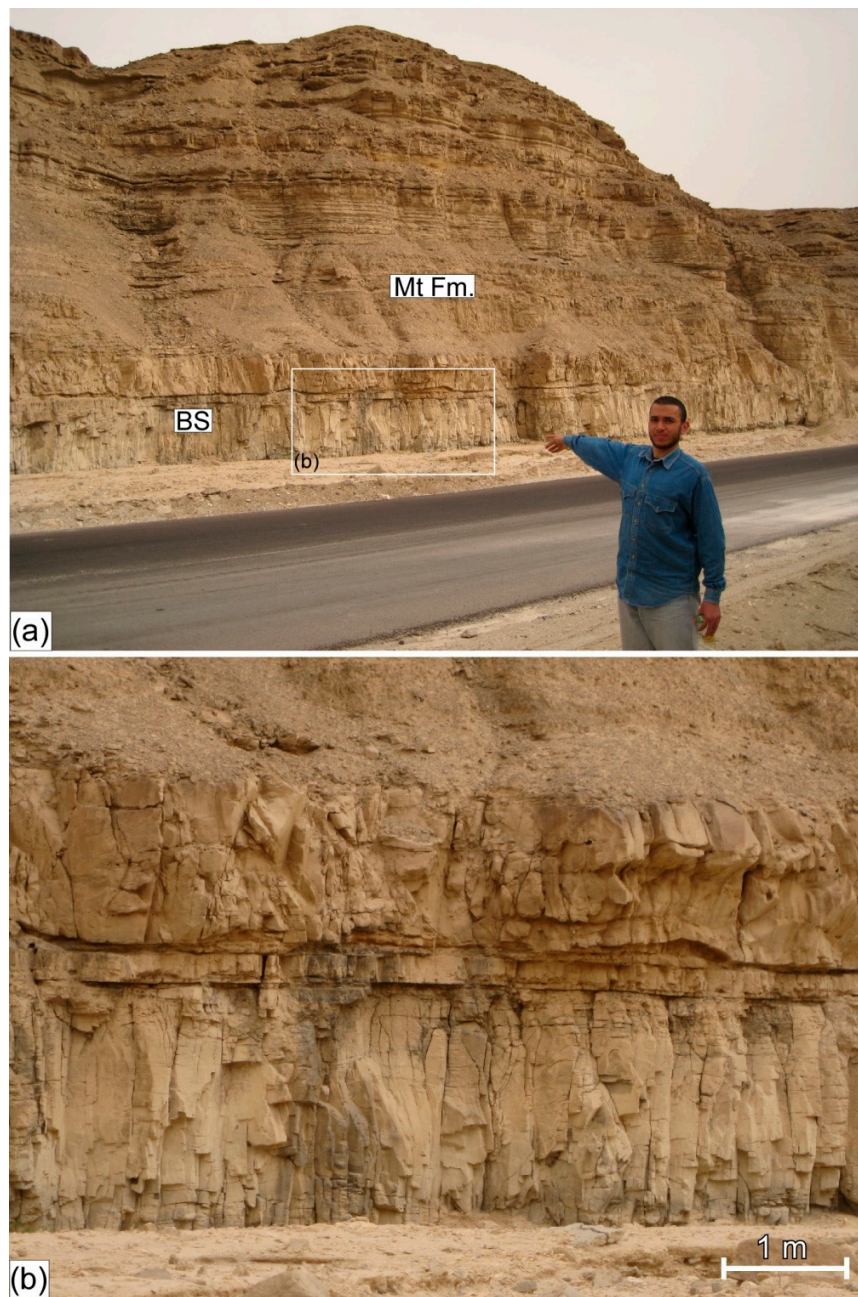


**Figure 6.** (a) General view of the horizontally bedded, clastic-dominated Matulla Formation (Mt Fm.) intruded by a 2 m thick basaltic sill (BS) at the entrance of Wadi Matulla. The man's height is 175 cm. (b) A close-up view of inset (b) in (a) showing a well-developed columnar jointing in the basaltic sill.

### 3. Methodology

#### 3.1. Total Organic Carbon (TOC)

TOC measurements were carried out on six samples that were collected from the Sudr Chalk at different distances from, and in a direction perpendicular to, the dyke (Table 1). The location of the samples with respect to the dyke and the country rock is shown in Figure 1.

**Table 1.** Total organic carbon (TOC) values, average temperatures, and colors of the samples from the Wadi Matulla area. (D: distance in meters from the dyke, see Figure 2c, TOC: Total Organic Carbon, T °C: Temperature in celsius).

Formation Name	Sample No.	Color	D (m)	TOC (wt %)	T (°C)
Sudr	1	White	3	0.1	450–500
	2	Black	5	2.71	>300
	3	Brownish grey	15	0.52	200–300
	4	Light brown	150	0.43	120–200
	5	Dark brown	160	1.57	120–200
	6	Greyish brown	180	0.32	120–200

### 3.2. Sample Preparation and TOC Measurement

The samples were mechanically pulverized to fine-grained (0.125–0.0625 mm) particles using the particle size analysis procedure. Applying the coning and quartering technique, a representative weight (50 g) of each sample was soaked in hydrochloric acid for 24 h to eliminate the carbonate fractions. To remove the resistant iron and magnesium carbonate, the samples were heated for two hours at 70 °C. The samples were then washed several times in distilled water to remove the remaining acid. To eliminate the chloride, the samples were washed in distilled water at 100 °C. The samples were filtered and the insoluble residue (IR), the sample fraction that was not eliminated by the acid treatment, was dried in an oven at 65 °C for three hours. The IR was weighed and ready for TOC measurements.

The TOCs were measured using the LECO analyzer SC-144 DR housed in the Egyptian Petroleum Research Institute (EPRI). The apparatus used is an oven that supplies a temperature of up to 1350 °C in an oxygen atmosphere to achieve a super dry condition. The technique depends on measuring the concentration of the carbon (CO<sub>2</sub>) expressed in weight percent. Assuming a complete elimination of the carbonates during the acid treatment, the IR is calculated in percent following the equation below:

$$IR = (DM/TM) \times 100 \quad (1)$$

where DM is the weight of the decarbonated sample and TM is the total weight of the sample before the acid treatment.

## 4. Results

### 4.1. The Petrography

#### 4.1.1. The Sudr Formation

Petrographically, five limestone microfacies were recognized: foraminiferal wackestone, foraminiferal packstone, chertified limestone with iron concretions, ferruginous mudstone, and dolostone [65–68]. They were very rich in allochems of benthic and planktonic foraminifera (Figure 7a–c), together with a few green algae (charophytes) and calcispheres. The benthic outnumbered the planktonic foraminifera, and included essentially miliolids, whereas the globigerinids were the typical planktonic foraminifera encountered. Other skeletal allochems such as ostracods and echinoid spines were recognized. All the allochems were tightly packed and cemented by a mosaic of spary calcite. Detrital components such as glauconitic grains were not uncommon. The biodiversity of deep planktonic and shallow benthic foraminifera together with the other skeletal allochems and glauconitic grains suggest mid- to outer-shelf setting [69]. Moreover, the calcispheres were typical of off-shelf water where turbulence is minimal, allowing the pelagic settling and accumulation of planktonic foraminifera-rich ooze ([70], and references therein).



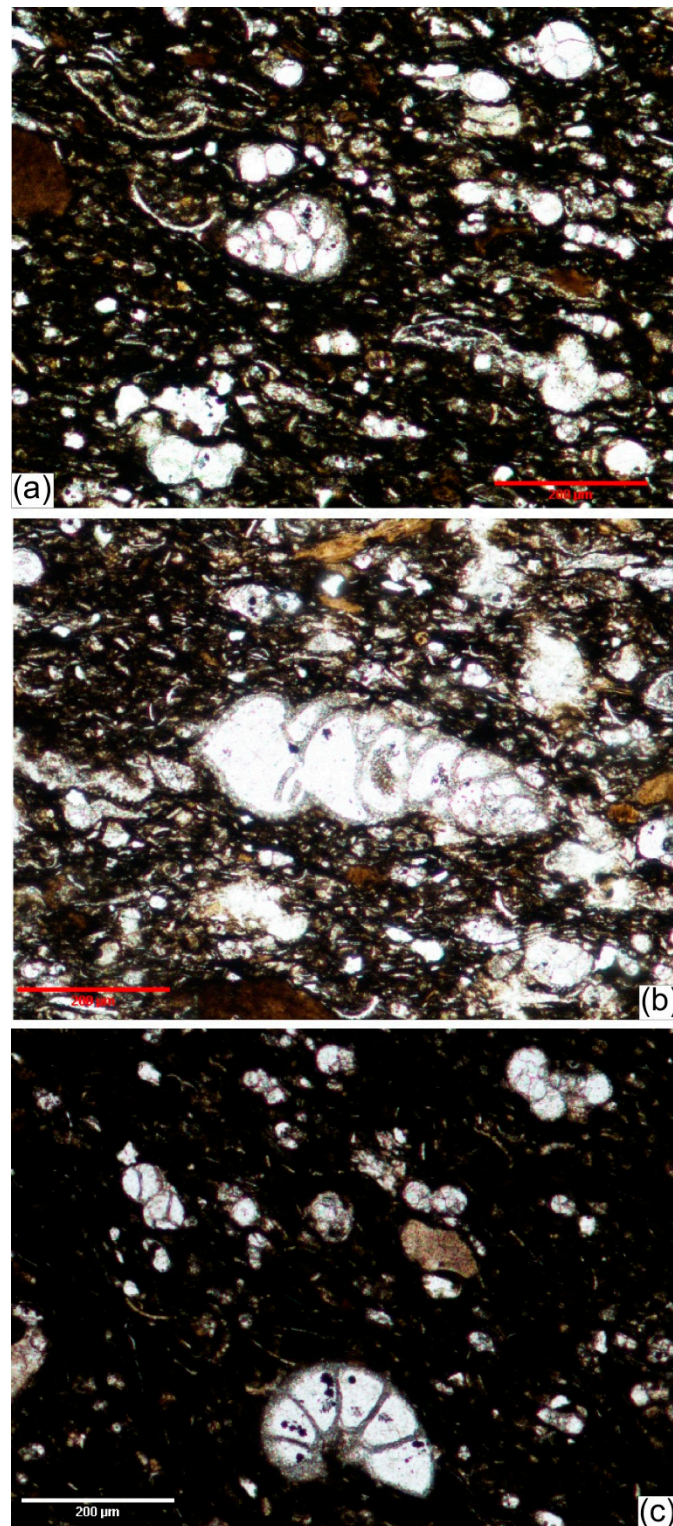


**Figure 7.** (a,b) Photomicrographs of organic matter-rich ferruginated mud hosting biserial calcareous benthic foraminifera and a few Ostracode carapaces, some of which terminate with a fishhook-like valve. (c) Wackestone (biomicrite) with planktonic (globigerinid) and multiple-chambered benthic foraminifera.

#### 4.1.2. The Basalt

The basaltic dyke is vitrophyric composed of subhedral to euhedral phenocrysts of sericitized plagioclase, fresh to partially altered olivine, and a few clinopyroxene crystals floating in a



cryptocrystalline to glassy ground mass (Figure 8a–c). Accessory phases include Fe-oxides and apatite. The rocks in general show porphyritic texture (Figure 8c). The vitrophyric texture (Figure 8) indicates the rapid cooling. The basalt shows Fe-enrichment, is silica oversaturated, enriched in the incompatible elements and depleted in the compatible elements [9,52]. For a detailed geochemical analysis of the dyke, the reader is referred to Shallaly et al., (2013) and El-Bialy et al., (2017) [9,52].

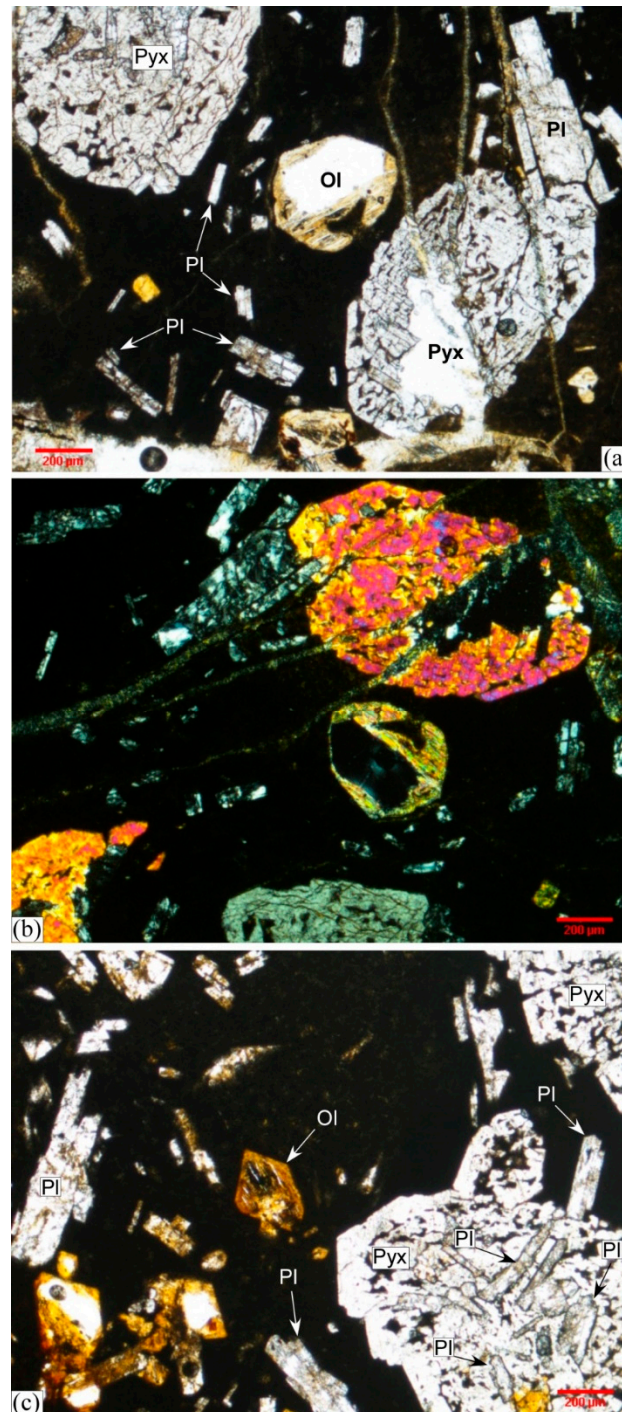


**Figure 8.** Photomicrograph in (a) PPL (plane polarized light) and (b) XPL (crossed polarized light) showing olivine (Ol), pyroxene (Pyx) and plagioclase (Pl) phenocrysts floating in a vitrophyric groundmass. (c) Olivine basalt preserving ophitic and subophitic textures.

#### 4.2. The Thermal Effect of the Dyke

The heat transferred from the hot lava caused a pronounced thermal effect on the Sudr Chalk. The thermal effect decreases dramatically away from the igneous body, and is traceable at the macroscopic, mesoscopic, and microscopic scales.

##### 4.2.1. The Baked Zone

A baked zone (BZ) of thermally affected Sudr Chalk is developed macroscopically on both sides of the dyke (Figures 2b,c, 9 and 10). The BZ has an irregular outline (Figures 2, 9a and 10) with an asymmetrical outcrop width ranging from 45 m to 160 m and from 10 m to 30 m along the western and the eastern sides of the dyke, respectively (Figure 2b,c). The Sudr Chalk in the baked zone shows, in general, a considerable variation in color ranging from black, in the close vicinity to the dyke (Figure 3d), to grey and brown, away from the dyke (Figures 9 and 10). However, heterogeneity at the mesoscopic scale in the close vicinity to the dyke is also recorded. Compositional and textural zonation within a one-meter-wide exposure of the Sudr Chalk is shown by the alternation of fine-grained black, coarse-grained grey and coarser-grained white zones (Figure 9c). The width of the baked zone implies high porosity and permeability of the rock. Apart from the primary porosity, the intense faulting and fracture systems (Figure 3b–d) that accompanied the rifting events of the GOS may have played a significant role in increasing the secondary porosity of the rock. However, detailed petrophysical analysis and microfacies study of the Sudr chalk, in the study area, are beyond the scope of this research.

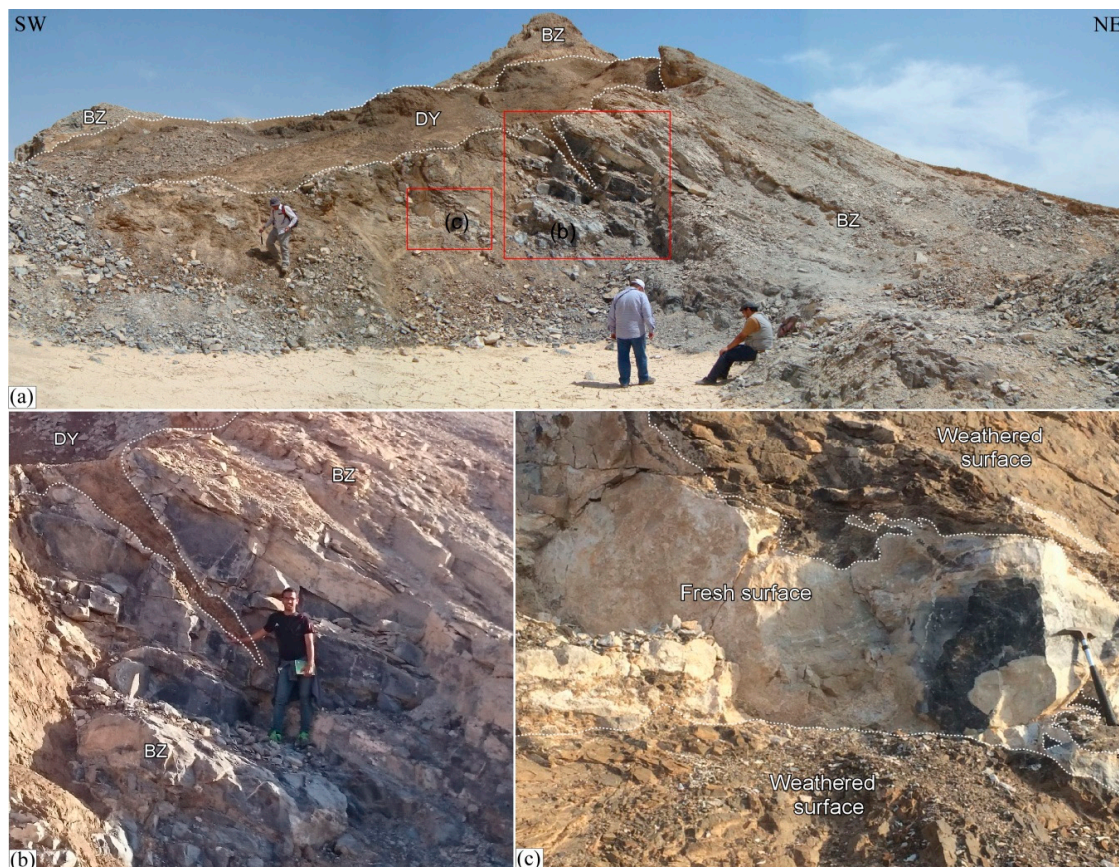


**Figure 9.** (a) Field photograph showing the dyke (DY) cutting through and having offshoots into the Sudr Chalk forming a baked zone (BZ) on both sides. (b) Close-up view of inset (b) in (a), showing an offshoot cutting across the country rock. (c) Close-up view of inset (c) in (a) showing compositional variation of the baked zone in the close vicinity of the dyke.

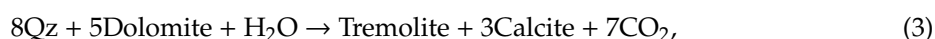




**Figure 10.** Panoramic view showing a N–S-trending grey-colored baked zone formed on the eastern side of the dyke cutting through the snow white-colored Sudr Chalk. (BZ: baked zone; DY: dyke, SUD: Sudr Chalk; UDZ: undisturbed zone).

#### 4.2.2. The Thermal Aureole

Mesoscopically, offshoots and veins of the dyke cut across the Sudr Chalk (Figure 9a,b). At the microscopic scale, veins and veinlets of the dyke cut through and engulf parts of the host rock (Figures 11a and 12a). Relics of the latter are present as isolated patches within the dyke. A very narrow, <10 centimeters wide, contact aureole is developed in the Sudr Chalk at its immediate contact with the dyke. The aureole contains the assemblage talc + tremolite + calcite + quartz + dolomite (Figures 10 and 11), that formed following the equations below:



The assemblage defines the lower and upper limits of tremolite and talc, respectively. The latter two phases coexist at a metamorphic temperature of about 500 °C marking the lower hornblende hornfels facies [71].

The intrusion of the dyke most likely occurred at very shallow levels. Figure 7 shows well-preserved microfossils in a very fine groundmass with a weakly defined preferred orientation, which suggests that the sediments experienced some compaction prior to the intrusion of the dyke. However, the fact that many microfossils preserve their spherical shape (Figure 7c) suggests that the amount of compaction was minimal. Moreover, the organic matter away from the dyke is immature and very well preserved, suggesting that the ambient temperature at the time of the dyke emplacement was very low (<100 °C). These observations suggest that the main controls on the mineral assemblage in the thermal aureole were the temperature of intrusion and the activity of H<sub>2</sub>O and CO<sub>2</sub>. At low pressure (≤ 1 kbar), the appearance of talc by Reaction (1) occurs at approximately 300 ± 50 °C, whereas the first appearance of tremolite occurs at approximately 350 ± 50 °C. Under these conditions, tremolite is replaced by diopside between 450 and 500 °C [71–74]. The lack of diopside in the mineral assemblage suggests that the maximum temperature at the dyke contact was ~500 °C.

Consequently, the temperature of the dyke at the time of intrusion can be inferred from the metamorphic mineral assemblage developed in the contact aureole. Outside the aureole, the thermal effect is restricted only to the recrystallization and coarsening of calcite crystals having typical polygonal texture with straight grain boundaries approaching equilibrium texture (Figure 11a). However, even at the microscopic scale, the latter texture is not homogeneously developed.



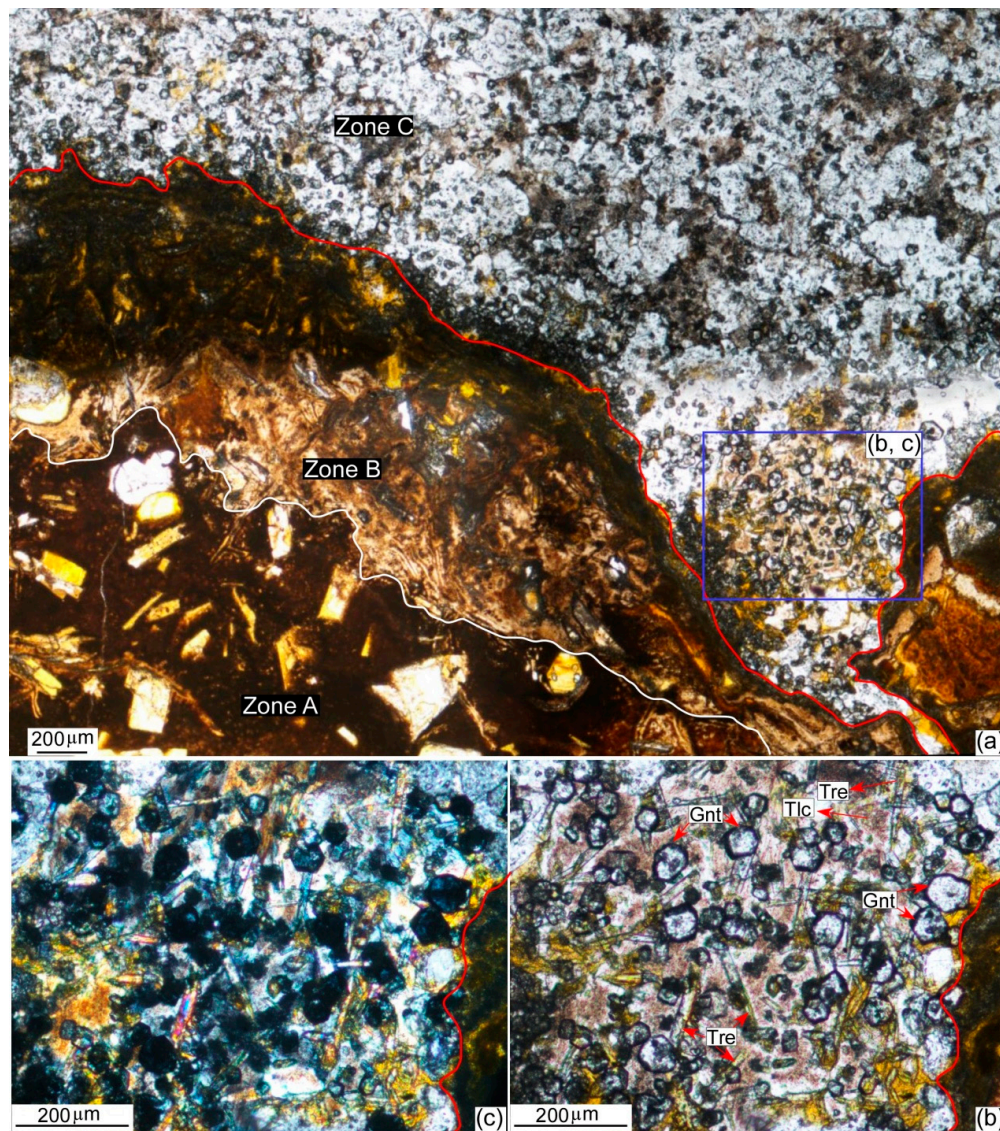


**Figure 11.** (a) Photomicrograph showing the development of metasomatized and metamorphic zones (zones B and C, respectively) in contact with the vitrophyric basalt (zone A). (b) Plane Polarized Light (PPL) and (c) Crossed Polarized Light (XPL) of inset (b,c) in (a) showing the growth of the metamorphic assemblage tremolite (Tre) and talc (Tlc), and the metasomatic garnet (Gnt) in zone C.



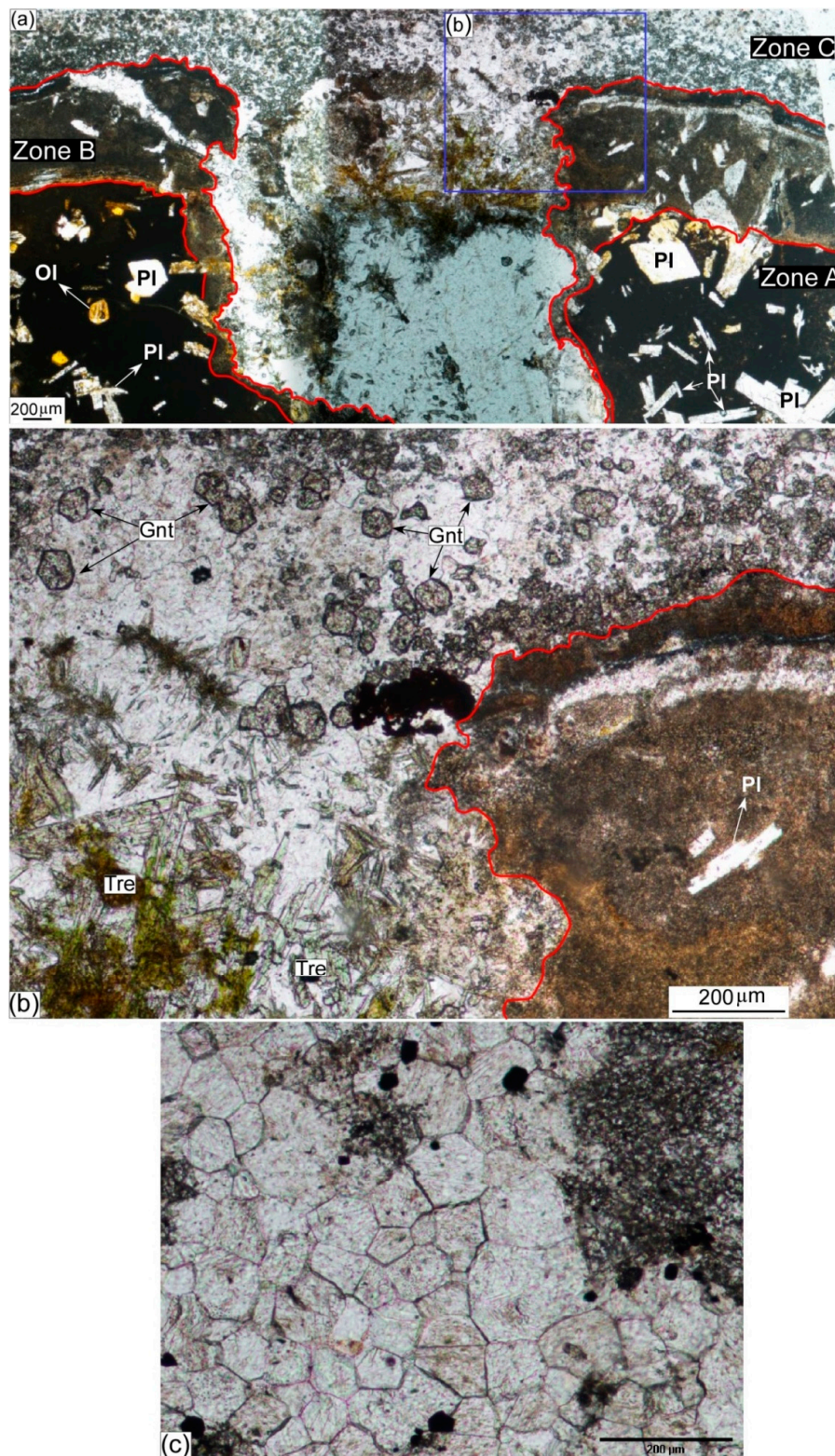


**Figure 12.** (a) Photomicrograph showing the metasomatic (zone B) and metamorphic (zone C) zones developed in contact with the vitrophyric basalt (zone A). (b) Close-up view of inset (b) in (a) showing the growth of the metamorphic assemblage tremolite and talc, and the metasomatic garnet in zone C. (c) Photomicrograph of a recrystallized limestone exhibiting equilibrium texture.

#### 4.2.3. The Metasomatic Effect

Metasomatism, the transfer of elements via circulating fluids between the lava and the host rock, is evidenced at the microscopic scale by the growth of new phases and the alteration of old ones. The former situation is evidenced by the very localized (at the scale of the thin section) growth of fine-grained garnet porphyroblasts (Figures 11 and 12). Close to the contact, the garnet crystals are generally coarser in grain size and idioblastic to sub-idioblastic, whereas further away from the contact they are generally represented by xenoblastic finer-grained crystals and aggregates. However, due to the unequal distribution of heat within the host rock, some coarser-grained idioblastic porphyroblasts are recorded away from the contact as well.

The garnets crystals are spatially related to the metamorphic assemblage tremolite + talc. However, the lack of the essential components for the garnet to grow (e.g., alumina) from the host carbonate rock implies a transfer of such component(s) from an external source, the dyke in our case. Consequently, we advocate for the metasomatic origin of the garnet. If this is accepted, the skarn-like garnets that are locally grown within a chalky limestone host rock are most probably grossular/hydrogrossular in composition. Furthermore, since the garnet coexists with and is in a very close spatial relation to the above-mentioned metamorphic assemblage, it is reasonable to suggest that the garnet has grown contemporaneously with, and in the stability field of, the metamorphic assemblage ( $\sim 500^\circ\text{C}$ ). Contact metasomatically grown garnets are well documented in the literature [75–77].

Coarse-grained calcite filling veins and veinlets that cut through the dyke is another example of growth of new phases. Some of the veins contain a few garnet crystals, implying formation in the stability field of garnet. Iron supplied by the basic lava is another form of the metasomatic process. It was carried in the hydrothermal solution that invaded the host rock through a net of veins and veinlets (Figure 13a,b). The iron filled the available spaces in the shells of the different fauna, and partially to completely replaced the shells and shell fragments (Figure 13b–d). Corona-like texture where Fe-carbonate is formed at the contact of the newly crystallized garnet with the carbonate country rock (calcite and/or dolomite) is also common.

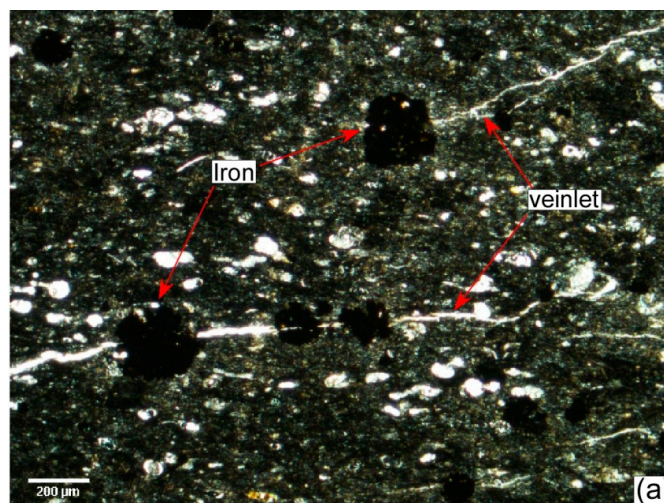
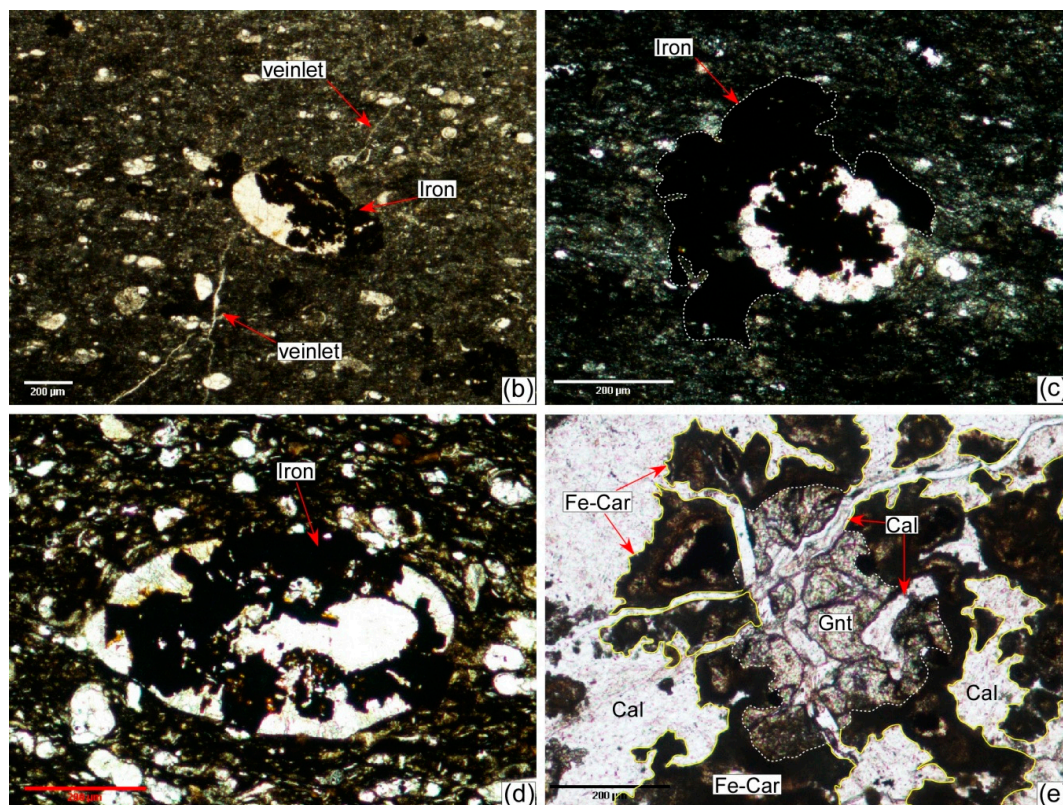


Figure 13. Cont.





**Figure 13.** (a) Iron-rich carbonized/carbon-rich chalky limestone (wackestone to packstone) with abundant calcispheres. The iron is spatially related to the veinlets that cut through the rock. (b) Calcisphere partially replaced by iron that is spatially related to veinlets cutting through chalky limestone (wackestone to packstone). Iron-rich carbonized chalky limestone showing calcareous algae (c) and skeletal fragment (d) in advanced stages of iron replacement. (e) Corona-like texture developed in marble. Iron-rich carbonate zone developed at the contact between the garnet and carbonate. (Cal: calcite, Gnt: garnet, Car: carbonate, Fe-Car: iron-rich carbonate).

Alteration of some existing phases is recognized in a few millimeter-thick zones of metasomatized basalt (Figures 11, 12 and 14). In contrast to the original basalt where the plagioclase phenocrysts are fresh to partially altered (Figure 14a, zone A), the phenocrysts in the hybrid zone are intensively saussuritized (Figure 14, zone B) implying the interaction of plagioclase with a hydrothermal solution with a significant mass transfer between the two neighboring systems. Interaction of the plagioclase phenocrysts with the calcium released from the carbonate rock into the hydrothermal solution cannot be ruled out. The latter conclusion is supported by the fact that the ground mass in the metasomatized zone is relatively coarser in grain size than the vitrophyric ground mass of the basaltic dyke, and is composed of indistinguishable calcareous constituents (Figure 14, zone B).

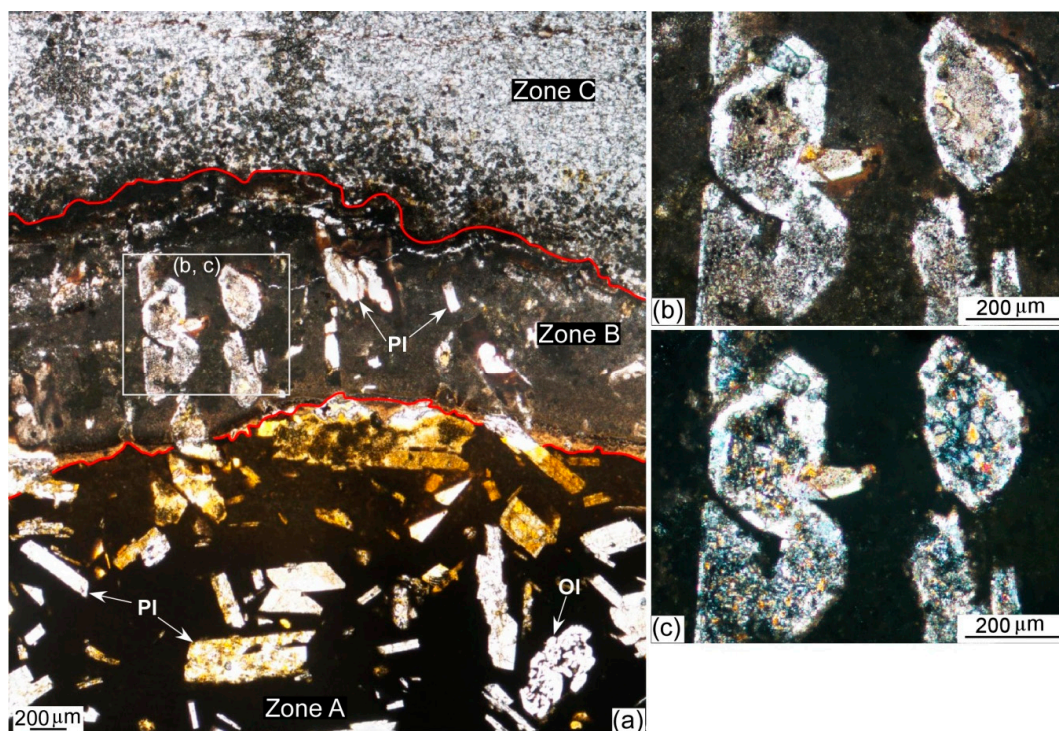


**Figure 14.** (a) Metasomatized basalt (zone B) preserving the porphyritic textures, and developed at the contact of the porphyritic, vitrophyric basalt (zone A) with the carbonate-rich country rock (zone C). (b) PPL and (c) XPL showing a close-up view of saussuritized plagioclase phenocrysts in the metasomatic zone B.

## 5. Discussion

### 5.1. The Source of Heat and Heat Transfer Mechanism

The dyke was the sole source of heat that caused the thermal effect. Heat transfer from a hot igneous body to the cold host rock can occur through three mechanisms: radiation, advection, and conduction. The latter depends largely on the thermal conductivity of the formation, which in turn depends on the temperature, pressure, porosity, composition, anisotropy of the formation, and properties of the pore-filling fluids [78]. Carbonate rocks, in general, have a good thermal conductivity compared to other rock types [79–82]. However, the thermal conductivity of a formation is inversely proportional to its porosity [83]. In the study area, faulting and the fracture systems that accompanied the rifting (Figure 3b–d) could have increased the secondary porosity of the chalky limestone and hence reduced its thermal conductivity (e.g., [83]). The disproportionality of the width of the baked zone (see Section 4.2.1) to that of the dyke and the reduced thermal conductivity of the host carbonate rocks imply the insignificant contribution of conduction in heat transfer. Similarly, due to the absence of a high-grade assemblage indicative of temperature greater than 600 °C, heat transfer by radiation is also excluded [82]. Consequently, we suggest advection was the most significant mechanism whereby heat transferred from the dyke to the host rock. Given that, a compelling question arises regarding the source of water that transferred the heat. Was it hot water expelled out of the dyke or cold pore-water within a water-saturated country rock, or both?

### 5.2. The Source of H<sub>2</sub>O

Primary mantle-derived basic magmas are generally anhydrous. In the study area, fractionated mantle sources with a significant and a minor crustal contribution have been interpreted for the parental lava of the basaltic rocks ([9] and [52], respectively). Partial melting at the garnet–spinel transition zone at a depth of 80–90 km has been interpreted [9]. El-Bialy et al., (2017), on the other



hand, suggested partial melting of asthenospheric amphibole-bearing garnet peridotite at a depth >70 km [52].

In the present study, the fresh character of, and the absence of any hydrous phases in the mantle-derived basaltic dyke imply its anhydrous nature (this study, [9,52]). Furthermore, similar interpretation has been approached geochemically by the significantly low values of the loss of ignition (LOI), 0.1–2.56, of the dyke [9]. However, implication of the intrusion of the dyke in a relatively hydrous state has been interpreted [52]. If the latter situation is accepted, however, it is very difficult to know exactly the water content in the dyke at the time of intrusion. Despite the contradictory interpretations [9,52], and assuming that the dyke was intruded in a hydrous state, we exclude the possibility that the dyke was the source of water that produced the thermal effect in the country rock for the following reasons: 1) the width of the baked zone is not proportional to that of the dyke, 2) volumetrically, the water content of a mantle-derived ~35 m wide (on average) basaltic dyke would be insignificant, and 3) high-grade metamorphic assemblages are absent at the immediate contact with the dyke. The latter reason can be further assisted by the cooling history of the dyke.

We, therefore, conclude that the pore-water in the water-saturated Sudr Chalk could have played a significant role in the heat transfer. However, groundwater upwelling cannot be ruled out. The groundwater could have been heated up by the dyke and found its way up into the Sudr Chalk through a system of rift-related faults and fractures.

### 5.3. Organic Matter, Organic Carbon (OC), and Total Organic Carbon (TOC)

Sources of organic matter in submarine sediments include marine phytoplankton, phytobentos, bacteria, and land-derived allochthonous materials [84–87]. The organic carbon (OC) concentration in the sediments varies from 0.1% to 5% depending on factors such as: (1) oxygen supply to the system, (2) preservation of the organic compounds, (3) mineral adsorption to certain compounds, (4) supply of terrigenous organic compounds, and (5) the rate of deposition of the sediments organic matter. The biogenic origin of coal and graphite has been the subject of much literature [88–91]. In petroleum geology, TOC is an indirect measure of the quality of source rocks [10]. Source rock potential in the GOS Rift, based on the TOC and pyrolysis results (S2), has been the subject of many studies [92–96]. An average TOC of 1.7% that reaches a maximum of 16% places the Sudr and Duwi formations (collectively known as the brown limestone) on top of the list of the richest source rocks in the northern and central provinces in the GOS [49,95,96]. In the study area, the Sudr Chalk with its prolific faunal content is the source of organic matter [90,91]. The measured TOCs of the samples (Table 1) cover the whole spectra of Peters's classification of source rock [10]. The samples range in color from black, dark brown, brownish grey, light brown, to greyish brown in a descending order of the TOC contents (Table 1 and Figure 13).

### 5.4. TOC, Thermal Maturation, and the Origin of the Baked Zone

Together with the other factors that affect the organic matter maturation (see Section 2), the time–temperature burial history of the organic matter-bearing sediments is of a prime importance [10]. For example, a slow rate of heating for a long duration at a convenient temperature favors source rock maturation to produce oil and/or gas. On the other hand, conditions of fast rate of heating and/or excessive temperature lead to the transformation of the organic matter directly into graphite. Detailed maturation indices of the source rock have not been carried out in this study. However, an evaluation of the thermal maturity of the organic matter and the temperature of maturation of the source rock in the study area can be inferred by correlating the colors of the isolated amorphous organic matter (AOM) and the phytoclasts (PhC) with the standard pollen/spore color chart of Pearson (1984) (Figure 15) [97]. The kerogens isolated from samples Mt4, Mt5, and Mt6 (TOC = 0.43, 1.57, and 0.32, respectively) range in color from light- to deep-brown. They are classified according to the thermal maturity of organic matter into mature samples with a maturation temperature in the range of 120–200 °C (Figure 15). Sample Mt3 has a TOC content of 0.52, and a deep-brown color

suggesting a mature to barren type of the thermal maturity standard, with a maturation temperature of 200–300 °C (Figure 15) Sample Mt2 (TOC = 2.71) is dark brown to black in color suggesting a dry type with a maturation temperature exceeding 300 °C (Figure 15) Sample Mt1 has the lowest TOC (0.1), is white in color, and barren in terms of organic matter (Figures 9c and 13). It represents an overmature metamorphic rock that is composed of the assemblage calcite, dolomite, chlorite, tremolite, and talc indicative of a high-grade metamorphic condition with a temperature in the range of 450–500 °C (Figure 15). The low TOC content and the white color of the sample, compared to the other samples, are attributed to the excessive metamorphic temperature that was high enough to completely burn the residual carbon.

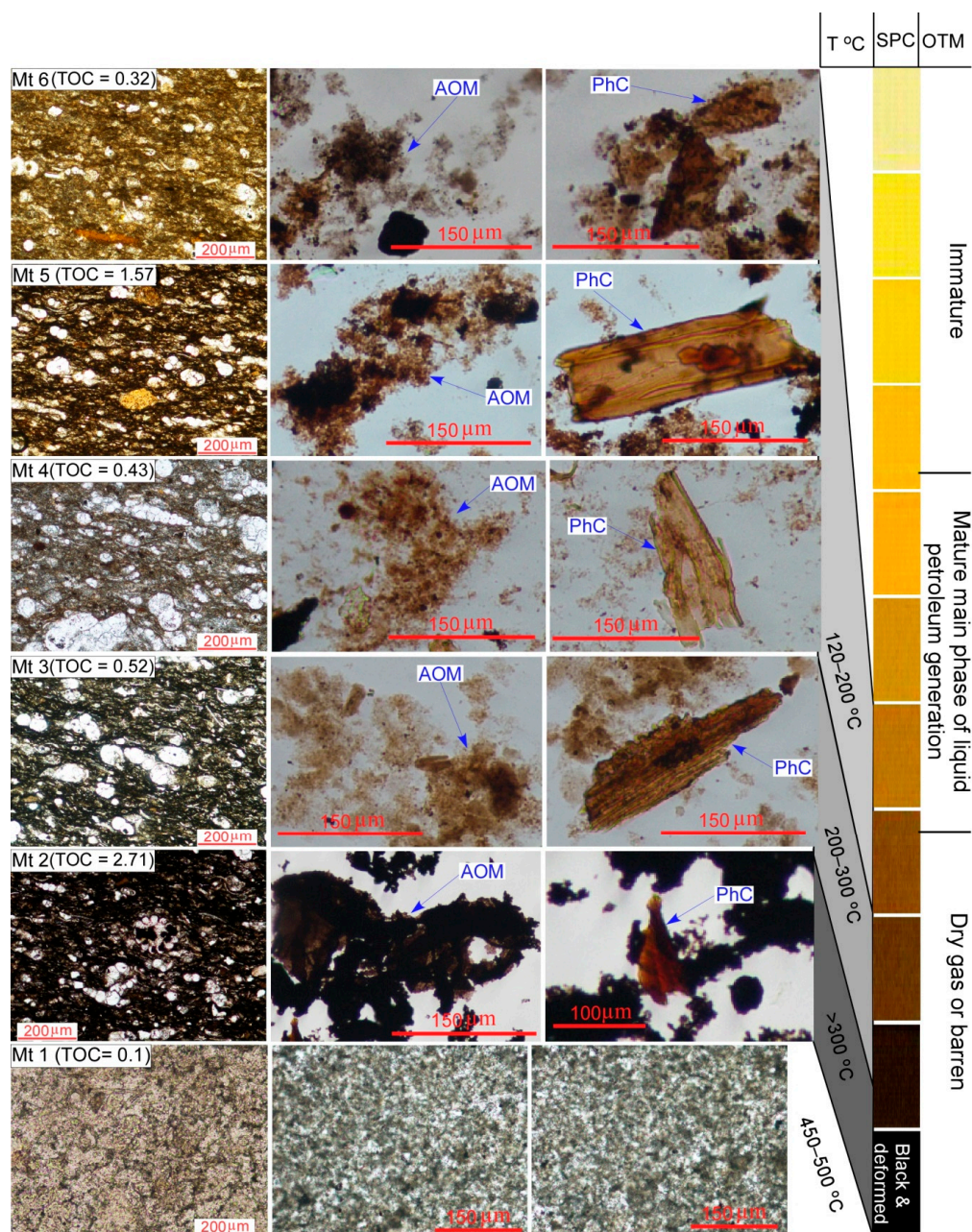


**Figure 15.** Schematic diagram showing the microfacies coloration, TOC, color of the amorphous organic matter (AOM), and phytoclasts (PhC), separated from the collected samples, in relation to the thermal maturation as compared to the standard Pollen/Spore Color Index (SPCI).



The change in the thermal maturation of organic matter and hence the difference in the TOC values within the baked zone can be attributed to the following: (1) the unequal dissipation of heat through the intruded rock, at the exposure scale, (2) the unequal distribution of the organic matter in the original rock, (3) certain anomalously hot spots in the rock, compared to the surroundings, and (4) the difference in the petrophysical properties, perhaps spot-by-spot, of the rock, and hence the efficiency of the heat transfer mechanism/mechanisms.

The different degrees of thermal maturation of the organic matter in the Sudr Chalk adjacent to the dyke turned the snow-white color of the chalk into shades of brown, grey, and black, and accounts for the formation of the baked zone in the Wadi Matulla area.

## 6. Implications of the Present Study

### *Local Maturation of Source Rock-Prone Formations in the GOS Region*

Compared to the hydrocarbons produced during maturation in normal subsiding basins, the extractable hydrocarbons, although from a localized source, are in some cases of economic value sufficient for commercial use [36]. The GOS Rift is considered to be the most oil-producing province in Africa and the Middle East [49]. Offshore oil fields produce more than 80% of the hydrocarbons. The sedimentary basins at great burial depths in the down-faulted blocks and downthrown sides of the rift-border faults were subjected to geothermal gradients high enough for the thermal maturation of the oil-prone source rocks to take place. However, at shallower burial depths in the upthrown sides of the major faults, the geothermal gradients decrease significantly to the point that thermal maturation of the source rocks cannot take place. The widespread syn-rift mafic sills, dykes, and small intrusive masses cutting through pre- and syn-rift source rocks in the upthrown blocks of the rift-border and -shoulder faults provide reasonable heat sources to compensate for the drastic decrease in the geothermal gradients. Consequently, these mafic intrusions at relatively shallow depths may either provide the thermal conditions favorable for maturation of the source rocks or get the latter into pre-maturation stages that would require, in the near future, minimal treatment for reasonable maturation. Hence, hydrocarbons can be produced from relatively shallow, oil-prone, type I kerogen-rich source rocks, as in the case of the present study, with greatly reduced costs provided that the subsurface configuration of the dyke is known through detailed subsurface and seismic data.

## 7. Conclusions

In the Wadi Matulla area, central Sinai, Egypt, a very high geothermal gradient accompanied by a rift-related Oligocene basaltic dyke resulted in the carbonization of the kerogene-bearing Upper Cretaceous Sudr Chalk over a 100 m wide baked zone. The Sudr Chalk varies in color (from brown, greyish brown, grey, to black) and consequently in TOC contents. The heat from the hot dyke was transferred through the water-saturated chalky limestone via advection. Transfer via upwelling of groundwater could be another possibility. Hornblende hornfels facies contact metamorphism, a few centimeters wide, as well as microscopic scale metasomatism were developed at the immediate contact with the dyke. The result of this research turns attention to the role of the mafic intrusions in the local maturation potential of source rocks at relatively shallow burial depths in the Gulf of Suez region. Therefore, it may open new channels, in the near future, to hydrocarbon extraction from shallower depths from around the rift-related intrusions.

**Author Contributions:** Conceptualization, A.S.A.A.S. and A.Q.S.; methodology, A.S.A.A.S., A.Q.S., M.M.A.F., S.M.H. and I.V.S.; validation, A.S.A.A.S., A.Q.S., and I.V.S.; investigation, A.S.A.A.S., A.Q.S., S.M.H.; data curation, A.S.A.A.S.; writing—original draft preparation, A.S.A.A.S., and S.M.H.; writing—review and editing, A.S.A.A.S., S.M.H., and M.M.A.F.; visualization, A.S.A.A.S., and A.Q.S.

**Funding:** This research received no external funding.

**Acknowledgments:** The authors would like to thank A. Maky, Egyptian Petroleum Research Institute, for the facilities offered for the TOC measurements and palynomorph analysis, and for the comments, suggestions and

invaluable discussions. Thanks go to Z. Abdullah, M. Selim and A. Zayed, Geology Department, Beni-Suef University, Egypt, and A. Maurice, Geology department, Helwan University, Egypt, for the fruitful discussions. I. Abdel Gayed and Y. Salam, Geology Department, Beni-Suef University, Egypt, are greatly acknowledged for helping in the identification of some benthic and planktonic foraminifera. We would like to thank anonymous reviewers for critical comments and suggestions that greatly improved the manuscript. Heather Wu is greatly acknowledged for editorial handling.

**Conflicts of Interest:** The authors declare no conflict of interest.

## References

1. Palumbo, F.; Main, I.G.; Zito, G. The thermal evolution of sedimentary basins and its effect on the maturation of hydrocarbons. *Geophys. J. Int.* **1999**, *139*, 248–260. [\[CrossRef\]](#)
2. Roberts, L.N.R.; Lewan, M.D.; Finn, T.M. Burial History, Thermal Maturity, and Oil and Gas Generation History of Petroleum Systems in the Southwestern Wyoming Province, Wyoming, Colorado, and Utah. In *Petroleum Systems and Geologic Assessment of Oil and Gas in the Southwestern Wyoming Province, Wyoming, Colorado, and Utah*, 1st ed.; USGS: Denver, CO, USA, 2005.
3. Grobe, A.; Littke, R.; Sachse, V.; Leythaeuser, D. Burial history and thermal maturity of Mesozoic rocks of the Dolomites, Northern Italy. *Swiss J. Geosci.* **2015**, *108*, 253–271. [\[CrossRef\]](#)
4. Simandl, G.J.; Paradis, S.; Akam, C. Graphite deposit types, their origin, and economic significance. In *Symposium on Strategic and Critical Materials*; British Columbia Geological Survey: Victoria, BC, Canada, 2015.
5. Beyssac, O.; Brunet, F.; Petitet, J.P.; Goffe, B.; Rouzaud, J.N. Experimental study of the microtextural and structural transformation of carbonaceous material under pressure and temperature. *Eur. J. Min.* **2003**, *15*, 937–951. [\[CrossRef\]](#)
6. Buseck, P.R.; Beyssac, O. From organic matter to graphite: graphitization. *Elements* **2014**, *10*, 421–426. [\[CrossRef\]](#)
7. El-Barkooky, A.N.; El-Araby, A. The Tertiary Red Beds of Abu Zenima area, West Central Sinai, Egypt: Their Stratigraphy and Sedimentology. In *Proceedings of the 4th Geology of the Arab World*, Cairo University, Cairo, Egypt, 1998; pp. 621–642.
8. El-Barkooky, A.N.; El-Araby, A.; Gaupp, R. Early Syn-Rift Deposition of alluvial-lacustrine facies in Wadi Nukhul, West Central Sinai. *Egypt. J. Geol.* **2006**, *50*, 141–169.
9. Shallaly, N.A.; Beier, C.; Haase, K.M.; Hammed, M.S. Petrology and geochemistry of the Tertiary Suez rift volcanism, Sinai, Egypt. *J. Volcan. Geother. Res.* **2013**, *267*, 119–137. [\[CrossRef\]](#)
10. Peters, K.E. Guidelines for Evaluating Petroleum Source Rocks using Programmed Pyrolysis. *Aapg Bull.* **1986**, *70*, 318–329.
11. Bosworth, W. Geological Evolution of the Red Sea: Historical Background, Review, and Synthesis. In *The Red Sea*; Rasul, N.M.A., Stewart, I.C.F., Eds.; Springer Earth System Sciences: Berlin/Heidelberg, Germany, 2015; pp. 45–78. [\[CrossRef\]](#)
12. Simoneit, B.R.T.; Brenner, S.; Peters, K.E.; Kaplan, I.R. Thermal alteration of Cretaceous black shale by diabase intrusions in the eastern Atlantic. Part II. Effects on bitumen and kerogen. *Geochim. Cosmochim. Acta* **1981**, *45*, 1581–1602. [\[CrossRef\]](#)
13. Akiyama, M.; Hirata, S.; Ujiie, Y. Thermal alteration of kerogen by basalt dykes intruded in the Oligocene Poronai Formation, Hokkaido, Japan. *J. Fac. Sci.* **1979**, *19*, 149–156.
14. Schiener, E.J.; Perregaard, J. Thermal maturation of organic matter by a thick basaltic sill in Upper Cretaceous shales, Svartenhuk Halve, Central West. Greenland. *Greenl. Geol. Surv.* **1981**, *102*, 16.
15. Clayton, J.L.; Bostick, N.H. Temperature effects on kerogen and on molecular and isotopic composition of organic matter in Pierre Shale near an igneous dike. *Org. Geochem.* **1986**, *10*, 135–143. [\[CrossRef\]](#)
16. Bishop, A.N.; Abbott, C.D. Vitrinite reflectance and molecular geochemistry of Jurassic sediments: The influence of heating by Tertiary dyke (northwest Scotland). *Org. Geochem.* **1995**, *22*, 165–177. [\[CrossRef\]](#)
17. Galushkin, Y.I. Thermal effects of igneous intrusions on maturity of organic matter: A possible mechanism of intrusion. *Org. Geochem.* **1997**, *26*, 645–658. [\[CrossRef\]](#)
18. Worden, R.H.; Smalley, P.C.; Cross, M.M. The influence of rock fabric and mineralogy on thermochemical sulfate reduction: Khuff Formation. *Abu Dhabi. J. Sed. Res.* **2000**, *70*, 1210–1221. [\[CrossRef\]](#)
19. Worden, R.H.; Smalley, P.C.; Barclay, S.A. H<sub>2</sub>S and diagenetic pyrite in North Sea sandstones: due to TSR or organic sulphur compound cracking? *J. Geochem. Explor.* **2003**, *78–79*, 487–491. [\[CrossRef\]](#)



20. Stewart, A.K.; Massey, M.; Padgett, P.L.; Rimmer, S.M.; Hower, J.C. Influence of a basic intrusion on the vitrinite reflectance and chemistry of the Springfield (No. 5) coal, Harrisburg, Illinois. *Int. J. Coal Geol.* **2005**, *63*, 58–67. [[CrossRef](#)]
21. Wang, D.; Lu, X.; Zhang, X.; Xu, S.; Hu, W.; Wang, L. Heat-model analysis of wall rocks below a diabase sill in Huimin Sag, China compared with thermal alteration of mudstone to carbargilite and hornfels and with increase of vitrinite reflectance. *Geophys. Res. Lett.* **2007**, *34*, L16312. [[CrossRef](#)]
22. Mastalerz, M.; Drobnia, A.; Schimmelmann, A. Changes in optical properties, chemistry, and micropore and mesopore characteristics of bituminous coal at the contact with dikes in the Illinois Basin. *Int. J. Coal Geol.* **2009**, *77*, 310–319. [[CrossRef](#)]
23. Schimmelmann, A.; Mastalerz, M.; Gao, L.; Sauer, P.E.; Topalov, K. Dike intrusions into bituminous coal, Illinois Basin: H, C, N, O isotopic responses to rapid and brief heating. *Geochim. Cosmochim. Acta* **2009**, *73*, 6264–6281. [[CrossRef](#)]
24. Aarnes, I.; Svensen, H.; Connolly, J.A.D.; Podladchikov, Y.Y. How contact metamorphism can trigger global climate changes: Modeling gas generation around igneous sills in sedimentary basins. *Geochim. Cosmochim. Acta* **2010**, *74*, 7179–7195. [[CrossRef](#)]
25. Aarnes, I.; Svensen, H.; Polteau, S.; Planke, S. Contact metamorphic devolatilization of shales in the Karoo Basin, South Africa, and the effects of multiple sill intrusions. *Chem. Geol.* **2011**, *281*, 181–194. [[CrossRef](#)]
26. Cao, X.; Chappell, M.; Schimmelmann, A.; Mastalerz, M.; Li, Y.; Hu, W.; Mao, J. Chemical structure changes in kerogen from bituminous coal in response to dike intrusions as investigated by advanced solid-state <sup>13</sup>C NMR spectroscopy. *Int. J. Coal Geol.* **2013**, *108*, 53–64. [[CrossRef](#)]
27. Brekke, T.; Krajewski, K.P.; Hubred, J.H. Organic geochemistry and petrography of thermally altered sections of the Middle Triassic Botneheia Formation on south-western Edgeøya, Svalbard. *Nor. Pet. Dir. Bull.* **2014**, *11*, 111–128.
28. Agirrezabala, L.M.; Permanyer, A.; Surez-Ruiz, I.; Dorronsoro, C. Contact metamorphism of organic-rich mudstones and carbon release around a magmatic sill in the Basque-Cantabrian Basin, western Pyrenees. *Org. Geochem.* **2014**, *69*, 26–35. [[CrossRef](#)]
29. Schofield, N.; Holford, S.; Millett, J.; Brown, D.; Jolley, D.R.; Passey, S.; Muirhead, D.; Grove, C.; Magee, C.; Murray, J.; et al. Regional magma plumbing and emplacement mechanisms of the Faroe-Shetland Sill Complex: Implications for magma transport and petroleum systems within sedimentary basins. *Basin Res.* **2015**, *29*, 41–63. [[CrossRef](#)]
30. Wang, D.; Manga, M. Organic matter maturation in the contact aureole of an igneous sill as a tracer of hydrothermal convection. *J. Geophys. Res. Solid Earth* **2015**, *120*, 4102–4112. [[CrossRef](#)]
31. Muirhead, D.K.; Bowden, S.A.; Parnell, J.; Schofield, N. Source rock maturation due to igneous intrusion in rifted margin petroleum systems. *J. Geol. Soc. Lond.* **2017**, *174*, 979. [[CrossRef](#)]
32. Reeckmann, S.A.; Mebberson, A.J. Igneous intrusions in the north-west Canning Basin and their impact on oil exploration. In *The Canning Basin*; Purcell, P.G., Ed.; Geological Society of Australia-Petroleum Exploration Society of Australia: Perth, Australia, 1984; pp. 389–399.
33. Hubred, J.H. Thermal Effects of Basaltic Sill Emplacement in Source Rocks on Maturation and Hydrocarbon Generation, Cand. Scient. Master's Thesis, University of Oslo, Oslo, Norway, 2006.
34. Vasquez, M.; Altenberger, U.; Romer, R.L. Neogene magmatism and its possible causal relationship with hydrocarbon generation in SW Colombia. *Int. J. Earth Sci.* **2009**, *98*, 1053–1062. [[CrossRef](#)]
35. Mark, N.J.; Schofield, N.; Pugliese, S.; Watson, D.; Holford, S.; Muirhead, D.; Brown, R.; Healy, D. Igneous intrusions in the Faroe Shetland basin and their implications for hydrocarbon exploration: New insights from well and seismic data. *Mar. Petro. Geol.* **2018**, *92*, 733–753. [[CrossRef](#)]
36. Muirhead, D.K.; Duffy, M.; Schofield, N.; Mark, N.; Rowe, M.D. *Making Oil from Magma*; Geological Society, London, Special Publications: London, UK, 2018; Volume 484.
37. Patton, T.L.; Moustafa, A.R.; Nelson, R.A.; Abdine, S.A. Tectonic evolution and structural setting of the Suez Rift. In *Interior Rift Basins*; Landon, S.M., Ed.; AAPG Memoir; American Association of Petroleum Geologists: Tulsa, OK, USA, 1994; Volume 59, pp. 7–55.
38. Khalil, S.M.; McClay, K.R. Tectonic evolution of the NW Red Sea–Gulf of Suez rift system. In *Non-Volcanic Rifting of Continental Margins: A Comparison of Evidence from Land and Sea*; Wilson, R.C.L., Whitmarsh, R.B., TAYlor, B., Froitzheim, N., Eds.; Geological Society, London, Special Publications: London, UK, 2001; Volume 187, pp. 453–473.

39. Bosworth, W.; Huchon, P.; McClay, K. The Red Sea and Gulf of Aden Basins. *J. Afr. Earth Sci.* **2005**, *43*, 334–378. [\[CrossRef\]](#)
40. Moustafa, A.R. Structural characteristics and tectonic evolution of the east-margin blocks of the Suez rift. *Tectonophysics* **1993**, *223*, 381–399. [\[CrossRef\]](#)
41. Bosworth, W. A high-strain rift model for the southern Gulf of Suez (Egypt). In *Hydrocarbon Habitat in Rift Basins*; Lambiase, J.J., Ed.; Geological Society, London, Special Publications: London, UK, 1995; Volume 80, pp. 75–102.
42. Gawthorpe, R.L.; Jackson, C.A.L.; Young, M.J.; Sharp, I.R.; Moustafa, A.R.; Leppard, C.W. Normal fault growth, displacement localisation and the evolution of normal fault populations: The Hammam Faraun fault block, Suez rift, Egypt. *J. Struc. Geol.* **2003**, *25*, 883–895. [\[CrossRef\]](#)
43. Jackson, C.A.L.; Gawthorpe, R.L.; Leppard, C.W.; Sharp, I.R. Riftinitiation development of normal fault blocks: insights from the Hammam Faraun fault block, Suez Rift, Egypt. *J. Geol. Soc.* **2006**, *163*, 165–183. [\[CrossRef\]](#)
44. Moustafa, A.M. Block faulting of the Gulf of Suez. In Proceedings of the 5th Exploration Seminar, Egyptian General Petroleum Company, Cairo, Egypt, 1976; p. 19.
45. Faulds, J.E.; Varga, R.J. The role of accommodation zones and transfer zones in the regional segmentation of extended terranes. In *Accommodation Zones and Transfer Zones: The Regional Segmentation of the Basin and Range Province*; Faulds, J.E., Stewart, J.H., Eds.; Geological Society of America: Boulder, CO, USA, 1998; Volume 323, pp. 1–45.
46. Moustafa, A.R. Structural setting and tectonic evolution of the northern Hammam Faraun block (Wadi Wasit Wadi Wardan area), eastern side of the Suez rift. *J. Univ. Kuwait-Sci.* **1996**, *23*, 105–132.
47. Moustafa, A.R. Controls on the Geometry of Transfer Zones in the Suez Rift and Northwest Red Sea: Implications for the Structural Geometry of Rift Systems. *AAPG Bull.* **2002**, *86*, 979–1002.
48. Younes, A.I.; McClay, K.R. Development of accommodation zones in the Gulf of Suez-Red Sea rift, Egypt. *Am. Assoc. Pet. Geol. Bull.* **2002**, *86*, 1003–1026.
49. Alsharhan, A.S. Petroleum geology and potential hydrocarbon plays in the Gulf of Suez rift basin, Egypt. *Aapg Bull.* **2003**, *87*, 143–180.
50. Kazmin, V.G.; Byakov, A.F. Magmatism and crustal accretion in continental rifts. *J. Afr. Earth Sci.* **2000**, *30*, 555–568. [\[CrossRef\]](#)
51. Bosworth, W.; McClay, K. Structural and stratigraphic evolution of the Gulf of Suez rift, Egypt: A synthesis. In *Peri-Tethys Memoir 6: Peri-Tethyan Rift/wrench Basins and Passive Margins*; Ziegler, P.A., Cavazza, W., Robertson, A.H.F., Crasquin-Soleau, S., Eds.; Mémoires du Muséum National d'Histoire Naturelle de Paris: Paris, France, 2001; Volume 186, pp. 567–606.
52. El-Bialy, M.Z.; Khalifa, I.H.; Omar, M.M. Continental intraplate volcanism in the Sinai subplate: The Oligo-Miocene basalts of the Gulf of Suez rift. *J. Afr. Earth Sci.* **2017**, *146*, 158–179. [\[CrossRef\]](#)
53. Said, R. Cenozoic. In *The Geology of Egypt*; Said, R., Ed.; CRC Press: Boca Raton, FL, USA, 1990; pp. 451–486.
54. Moustafa, A.R.; Abdeen, M.M. Structural setting of the Hammam Faraun block, eastern side of the Suez rift. *J. Univ., Kuwait Sci.* **1992**, *19*, 291–309.
55. Sharp, I.R.; Gawthorpe, R.L.; Underhill, J.R.; Gupta, S. Fault propagation folding in extensional settings: Examples of structural style and syn-rift sedimentary response from the Suez Rift, Egypt. *Geol. Soc. Amer. Bull.* **2000**, *112*, 1877–1899. [\[CrossRef\]](#)
56. Bastesen, E.; Braathen, A.; Skar, T. Comparison of scaling relationships of extensional fault cores in tight carbonate and porous sandstone reservoirs. *Pet. Geosci.* **2015**, *19*, 385–398. [\[CrossRef\]](#)
57. Barakat, M.G.; Darwish, M.; El Outefi, N.S. Eocene tectonostratigraphy and basin evaluation in the Gulf of Suez petroliferous province. In Proceedings of the 9th Egyptian General Petroleum Corporation, Petroleum Exploration and Production Conference, Cairo, Egypt, 1988; Volume 1, pp. 1–22.
58. Abu Khadra, A.M.; Youssef, E.A.A.; Refaat, A. Depositional environments and diagenesis of the Matulla Formation, Abu Zenima area, West-Central Sinai, Egypt. *Bull. Fac. Sci.* **1990**, *58*, 493–513.
59. Abdelhamid, M.A.M. Turonian-Santonian echinoids from Wadi Sudr and Wadi Matulla, west central Sinai. *Middle East Res. Cent. Ain Shams Univ. Earth Sci. Ser.* **1997**, *11*, 136–158.
60. Abdel-Gawad, G.I. Biostratigraphy and macrofossil assemblages of the Matulla Formation (Coniacian–Santonian), west central Sinai, Egypt. *Middle East Res. Cent. Ain Shams Univ. Earth Sci. Ser.* **1999**, *13*, 187–202.



61. Kora, M.; Hamama, H.; Sallam, H. Senonian macrofauna from West-Central Sinai: Biostratigraphy and Paleobiogeography. *Egypt. J. Paleontol.* **2002**, *2*, 235–258.
62. Shahin, A.M. Maastrichtian to Middle Eocene ostracodes from Sinai, Egypt: Systematics, biostratigraphy and paleobiogeography. *Rev. De PaléobiologieGenève* **2005**, *24*, 749–779.
63. Farouk, S. Maastrichtian carbon cycle changes and planktonic foraminiferal bioevents at Gebel Matulla, west-central Sinai, Egypt. *Cretac. Res.* **2014**, *50*, 238–251. [[CrossRef](#)]
64. Meneisy, M.Y. Vulcanicity. In *The Geology of Egypt*; Said, R., Ed.; Balkema, A.A.: Rotterdam, The Netherlands, 1990; pp. 157–172.
65. Folk, R.L. Practical petrographic classification of limestones. *AAPG Bull.* **1959**, *43*, 1–38.
66. Dunham, R.J. Classification of carbonate rocks according to depositional of texture 1. In *Classification of Carbonate Rocks—A Symposium*; Ham, W.E., Ed.; American Association of Petroleum Geologists: Tulsa, OK, USA, 1962; Volume 1, pp. 108–121.
67. Embry, A.F.; Klovan, E.J. Absolute water depth limits of Late Devonian paleoecological zones. *Geol. Rdsch.* **1972**, *61*, 672–686. [[CrossRef](#)]
68. Wilson, J.L. *Carbonate Facies in Geological History*; Springer: Berlin, Germany, 1975; p. 471.
69. Scholle, P.A.; Ulmer-Scholle, D.S. *A Color Guide to Petrography of Carbonate Rocks: Grains, Textures, Porosity, Diagenesis*, AAPG Memoir 77; The American Association of Petroleum Geologists: Tulsa, OK, USA, 2003.
70. Khalifa, M.A.; Farouk, S.; Hassan, A.M. Carbonate platform facies development of the Turonian Wata Formation in Central and Eastern Sinai. *Egypt. J. Afr. Earth Sci.* **2016**, *124*, 126–138. [[CrossRef](#)]
71. Bucher, K.; Frey, M. *Petrogenesis of Metamorphic Rocks*, 7th ed.; Springer: Berlin, Germany, 2002; p. 341.
72. Rice, J.M. Contact metamorphism of impure dolomitic limestone in the Boulder Aureole, Montana. *Contrib. Mineral. Petrol.* **1977**, *59*, 237–259. [[CrossRef](#)]
73. Holness, M.B. Fluid flow path and mechanisms of fluid infiltration in carbonates during contact metamorphism: The Beinn an Dubhaich aureole, Skye. *J. Meta. Geol.* **1997**, *15*, 59–70. [[CrossRef](#)]
74. Jamtveit, B.; Dahlgren, S.; Austrheim, H. High grade contact metamorphism of calcareous rocks from the Oslo Rift, Southern Norway. *Am. Mineral.* **1997**, *82*, 1241–1254. [[CrossRef](#)]
75. Stowell, H.H.; Menard, T.; Ridgway, C.K. Ca-metasomatism and chemical zonation of garnet in contact-metamorphic aureoles, Juneau Gold Belt, southeastern Alaska. *Can. Mineral.* **1996**, *34*, 1195–1209.
76. Kent, A.J.R.; Ashley, P.M.; Fanning, C.M. Metasomatic alteration associated with regional metamorphism: An example from the Willyama Supergroup, South Australia. *Lithos* **2000**, *54*, 33–62. [[CrossRef](#)]
77. Ranjbar, S.; Tabatabaei Manesh, S.M.; Mackizadeh, M.A.; Tabatabaei, S.H.; Parfenova, O.V. Geochemistry of major and rare earth elements in garnet of the Kal-e Kafi skarn, Anarak Area, Central Iran: Constraints on processes in a hydrothermal system. *Geochem. Inter.* **2016**, *54*, 423–438. [[CrossRef](#)]
78. Hurtig, E.; Brugger, H. Heat conductivity measurements under uniaxial pressure. *Tectonophysics* **1970**, *10*, 67–77. [[CrossRef](#)]
79. Lubimova, E.A.; Smirnova, E.V. Heat physical properties of rocks at high temperatures. In *Physical Properties of Rocks under High Pressure and Temperature*; Trans. of IV All-Union Congress: Tbilisi, Georgia, 1974; pp. 171–172. (In Russian)
80. Robertson, E.C. *Thermal Conductivity of Rocks*. U.S. Geological Survey Open File Report; USGS: Denver, CO, USA, 1979; pp. 79–356.
81. Kelemen, P.B.; Kikawa, E.; Miller, D.J. Drills into mantle peridotite along the mid-Atlantic ridge from 14°N to 16°N. In Proceedings of the Ocean Drilling Program, Rio de Janeiro, Brazil, 6 May–7 July 2004; Volume 30, pp. 14–19.
82. Clauser, C.E. Thermal conductivity of rocks and minerals. In *Rock Physics and Phase Relations: A Handbook of Physical Constants*; Ahrens, T.J., Ed.; American Geophysical Union: Washington, DC, USA, 1995; Volume 3, pp. 105–126.
83. Poelchau, H.S.; Baker, D.R.; Hantschel, T.; Horsfield, B.; Wygrala, B. Basin simulation and the design of the conceptual basin model. In *Petroleum and Basin Evaluation*; Welte, D.H., Horsfield, B., Baker, D.R., Eds.; Springer: Berlin, Germany, 1997; pp. 36–41.
84. Emeis, K.C.; Kvenvolden, K.A. Shipboard organic geochemistry on Joides Resolution. *ODP Tech. Notes* **1986**, *7*.
85. Lampitt, R.S.; Bett, B.J.; Kiriakoulakis, K.; Popova, E.E.; Ragueneau, O.; Vangriesheim, A.; Wolff, G.A. Material supply to the abyssal seafloor in the northeast Atlantic. *Prog. Oceanogr.* **2001**, *50*, 27–63. [[CrossRef](#)]

86. Goni, M.A.; O'Connor, A.E.; Kuzyk, Z.Z.; Yunker, M.B.; Gobeil, C.; Macdonald, R.W. Distribution and sources of organic matter in surface marine sediments across the North American Arctic margin. *J. Geophys. Res. Ocean.* **2013**, *118*, 4017–4035. [[CrossRef](#)]
87. Hunter, W.R.; Jamieson, A.; Huvenne, V.A.I.; Witte, U. Sediment community responses to marine vs. terrigenous organic matter in a submarine canyon. *Biogeosciences* **2013**, *10*, 67–80. [[CrossRef](#)]
88. Mancsuo, J.T.; Seavoy, R.E. Precambrian coal or anthraxolite: A source for graphite in high-grade schists and gneisses. *Econ. Geol.* **1981**, *65*, 273–298. [[CrossRef](#)]
89. Hollister, V.F. Origin of graphite in the Duluth Complex. *Econ. Geol.* **1980**, *75*, 764–766. [[CrossRef](#)]
90. Disssanayake, C.B. The Origin of graphite of Sri Lanka. *Org. Geochem.* **1981**, *3*, 1–7. [[CrossRef](#)]
91. Soman, K.; Lobzova, R.V.; Sivadas, K.M. Geology, genetic types, and origin of graphite in South Kerala, India. *Econ. Geol.* **1986**, *81*, 997–1002. [[CrossRef](#)]
92. Shaheen, A.N.; Shehab, M. Petroleum generation, migration and occurrence in the Gulf of Suez offshore, south Sinai. In Proceedings of the 17th Egyptian General Petroleum Corporation, Petroleum Exploration and Production, Cairo, Egypt, 1984; Volume 1, pp. 126–152.
93. Atef, A. Source rock evaluation of the Brown Limestone (upper Senonian), Gulf of Suez. In Proceedings of the 9th Egyptian General Petroleum Corporation; Petroleum Exploration and Production, Cairo, Egypt, 1988; Volume 1, pp. 256–275.
94. Moustafa, A.R.; Klitzsch, E.; Matheis, G.; Ganz, H. Origin and evaluation of hydrocarbons in the Gulf of Suez Basin, Egypt. In *Geoscientific Research in North East Africa*; Thorweihe, U., Schandelmeier, H., Eds.; CRC Press: Boca Raton, FL, USA, 1993; pp. 267–275.
95. Alsharhan, A.S.; Salah, M.G. Geology and hydrocarbon habitat in rift setting: Southern Gulf of Suez, Egypt. *Bull. Can. Petro. Geol.* **1994**, *42*, 312–331.
96. Alsharhan, A.S.; Salah, M.G. Geology and hydrocarbon habitat in rift setting: Northern and central Gulf of Suez, Egypt. *Bull. Canad. Pet. Geol.* **1995**, *43*, 156–176.
97. Pearson, D.L. *Pollen/Spore Colour “Standard”*; Version 2, Phillips Petroleum Company Exploration Projects Section; Phillips Petroleum Company, Privately distributed: Bartlesville, OK, USA, 1984.



© 2019 by the authors. Licensee MDPI, Basel, Switzerland. This article is an open access article distributed under the terms and conditions of the Creative Commons Attribution (CC BY) license (<http://creativecommons.org/licenses/by/4.0/>).